Viscosities and Densities of Binary Mixtures of Hexadecane with Dissolved Methane or Carbon Dioxide at Temperatures From (298 to 473) K and at Pressures up to 120 MPa

Malami Mohammed, Fausto Ciotta and J. P. Martin Trusler*

Department of Chemical Engineering, Imperial College London, South Kensington Campus, London SW7 2AZ, U.K.

* To whom correspondence should be addressed. E-mail: m.trusler@imperial.ac.uk

ABSTRACT

We report measurements of the viscosity and density of two binary mixtures comprising hexadecane with dissolved carbon dioxide or methane over the temperature range from (298.15 to 473.15) K and at pressures up to 120 MPa. The measurements were conducted at various mole fractions x of the light component as follows: x = (0, 0.0690, 0.5877 and 0.7270) for $x\mathrm{CO_2}$ + (1 - x)$\mathrm{C_{16}H_{34}}$ and x = (0, 0.1013, 0.2021, 0.2976 and 0.3979) for $x\mathrm{CH_4}$ + (1 - x)$\mathrm{C_{16}H_{34}}$. The viscosity and density measurements were carried out simultaneously using a bespoke vibrating-wire apparatus with a suspended sinker. With respect to the first mixture, the apparatus was operated in a relative mode and was calibrated in octane whereas, for the second mixture, the apparatus was operated in an absolute mode. To facilitate this mode of operation, the diameter of the centreless-ground tungsten wire was measured with a laser micrometer, and the mass and volume of the sinker were measured independently by hydrostatic weighing. In either mode of operation, the expanded relative uncertainties at 95 % confidence were 2 % for viscosity and 0.3 % for density. The results were correlated using simple relations that express both density and viscosity as functions of temperature and pressure. For both pure hexadecane and each individual mixture, the results have been correlated using the modified Tait equation for density, and the Tait-Andrade equation for viscosity; both correlations described our data almost to within their estimated uncertainties. In an attempt to model the viscosity of the binary mixtures as a function of temperature, density and composition, we have applied the extended-hard-sphere model using several mixing rules for the characteristic molar core volume. The most favourable mixing rule was found to be one based on a mole-fraction-weighted sum of the pure component molar core volumes raised to a power γ which was treated as an adjustable parameter. In this case, deviations of the experimental viscosities from the model were within ±25 %.

Keywords: Asymmetric mixtures; Carbon dioxide; Density; Hexadecane; High pressure; Methane; Viscosity.

1. INTRODUCTION

Continuing global population growth, increasing per-capita energy demand and depletion of conventional crude oil resources have stimulated research activities aimed both at maximizing the recovery of conventional crude oil and at enabling economic exploitation of unconventional hydrocarbon resources such as heavy and extra-heavy crude oils.

In the area of improved recovery of conventional petroleum resources, enhanced oil recovery via the injection of supercritical carbon dioxide (CO_2-EOR) has been employed in certain fields. In this technique, CO_2 is injected into a partially-depleted reservoir in order to boost pressure, increase sweep efficiency, solubilize residual hydrocarbons, reduce viscosity, and ultimately aid the recovery process. Similarly, economic production of heavy oil is often contingent upon viscosity reduction to facilitate flow in the reservoir, production wells, and transportation and processing facilities. In this context, injection of low-molecular weight hydrocarbons (*e.g.* CH_4, C_2H_6 C_3H_8 etc.) as solvents can be a convenient way of reducing viscosity. It must also be recognized that continued exploitation of hydrocarbon resources to meet growing energy demand while avoiding dangerous climate change is a massive challenge for the oil industry. Capture and storage of CO_2 in deep geological formations (carbon capture and storage, CCS) is a technology that has the potential to tackle CO_2 emissions from the combustion of fossil fuels. In CCS, as in CO_2-EOR, the captured CO_2 is injected into an underground reservoir for permanent storage. In this process, CO_2 contacts and mixes with hydrocarbons and other reservoir fluids. Thus CO_2-EOR, light solvent extraction of heavy oils, and CO_2 storage in depleted oil reservoirs all involve the formation of so-called asymmetric fluid mixtures, which comprise both light and heavy components. Furthermore, the engineering of these processes requires estimation of the thermophysical properties including the miscibility behavior, viscosity and density. Unfortunately, predicting the thermophysical properties, especially viscosity, of asymmetric mixtures is challenging.

Modeling tools suitable for predicting the viscosity of industrially-important asymmetric fluid mixtures are highly imperfect and the prediction of this property from pure component properties alone offers poor accuracy. For instant, Ciotta *et al*.[1, 2] showed that relative deviations of up to 60 % from experimental data could arise when estimating the viscosity of (CO_2 + squalane) from the hard-sphere model with the conventional mixing rule.[3] Moreover, the accuracy of existing predictive models generally deteriorates as the individual components of the mixture become more different in size and/or shape.

To address the problem of predicting viscosity, in particular for asymmetric mixtures, new modelling approaches may be required but a prerequisite is the availability of sufficient experimental data to parameterize and/or validate such models. Despite the importance of asymmetric mixtures, few data are available for the viscosity and density of representative mixtures. The situation is illustrated in Table 1 where we list the available literature data for the viscosity of mixtures of alkanes with either methane[4-24] or carbon dioxide.[5, 9, 25-35] The system methane + decane is something of an exception with experimental results reported by Lee and Eakin,[17] Knapstad *et al*.,[23] Dauge *et al.,*[18] Canet *et al*.,[19] Audonnet and Padua,[16] Gozalpour *et al.,*[20] Peleties,[21] and Daridon *et al*.[22] Few data are found for asymmetric mixtures of either methane or carbon dioxide with other hydrocarbons. The open literature also includes

little experimental data for the viscosity of mixtures of carbon dioxide with crude oils; Table 2 lists the data sources identified by the authors.[36-39]

In view of the deficiency of relevant published experimental data, we are measuring in our laboratory the viscosity of asymmetric mixtures of light molecules with both pure hydrocarbons and crude oils. The present work aims to fill the gaps in the literature by providing new data for the viscosity and density of binary mixtures of *n*-hexadecane with methane or carbon dioxide. We also explore the modelling of these system by means of the extended hard-sphere model,[40] with different mixing rules.

2. EXPERIMENTAL SECTION

2.1 Materials

The materials used in this work are detailed in Table 3. The purity of the *n*-hexadecane was investigated by gas chromatography-mass spectrometry (GC-MS). An estimated mass-fraction purity of w = 99.83 % was deduced from the chromatogram and the mass spectra of the impurities revealed that the remaining 0.17 % was likely predominantly *n*-nonadecane. The properties of the GC system used are listed in Table 4.

2.2 Apparatus

The density and viscosity measurements were carried out simultaneously using a bespoke vibrating-wire apparatus illustrated in Figure 1.[41] The centerless-ground tungsten wire (Metal Cutting Corp. New Jersey, USA) of nominal length 65 mm and nominal diameter 0.15 mm was clamped at the top and tensioned by a suspended aluminum sinker with a nominal mass of either 0.3 kg or 0.4 kg (two different sinkers were used in this work). The wire passed between the poles of a permanent magnet assembly with magnetic field strength of about 0.3 T at T = 298.15 K.

The instrument was operated in steady-state mode with a constant alternating current passing through the wire, exciting transverse oscillations. The electromotive force $V(f)$ developed across the wire was measured with a two-phase lock-in amplifier and data were gathered for a range of imposed driving frequency f in the vicinity of the fundamental transverse mode of oscillation. The resonance frequency of the wire is sensitive to the density of the fluid, primarily as a consequence of the buoyancy effect on the suspended sinker, while the width of the resonance curve is sensitive to the viscosity of the surrounding fluid.

Generally, $V(f)$ is the sum of two terms: the first, $V_1(f)$, arises from the electrical impedance of the stationary wire; whereas the second, $V_2(f)$, is the induced voltage arising from the movement of the wire in the magnetic field. The first term conforms to the following relation,

$$V_1(f) = a_0 + ia_1 + ia_2 f \quad , \tag{1}$$

where a_0, a_1, and a_2 are real constants; the second is given according to the working equation of Retsina *et al.*[42] as follows:

$$V_2(f) = \frac{i\Lambda f}{f_0^2 - f^2(\beta + 1) + if^2(\beta' + 2\Delta_0)}. \quad (2)$$

In equation (2), Λ is an amplitude, f_0 is the "buoyancy-adjusted" vacuum resonance frequency, Δ_0 is the vacuum decrement and β and β' account respectively for the added mass and viscous damping of the fluid surrounding the wire. The latter are given by

$$(\beta' + i\beta) = \frac{\rho}{\rho_w}\left[i + \frac{4i\,K_1\left(\sqrt{i\Omega}\right)}{\sqrt{i\Omega}\,K_0\left(\sqrt{i\Omega}\right)}\right], \quad (3)$$

where

$$\Omega = 2\pi f \rho R^2 / \eta. \quad (4)$$

Here, ρ and ρ_w are the densities of the fluid and the wire, K_n is the modified Bessel function of the second kind of order n, η is the viscosity of the fluid, and R is the radius of the wire.

The buoyancy-adjusted vacuum resonance frequency f_0 corresponds to the hypothetical situation of the wire in vacuum with the sinker immersed in the fluid. We model this system as an end-clamped stiff tensioned wire according to the relation discussed by Ciotta and Trusler,[43] which is as follows:

$$f_0 = \frac{1}{2L}\left[A\sqrt{\frac{(m - \rho V)g}{\rho_s \pi R^2}} + \sqrt{\frac{ER^2}{\rho_s L^2}} + \left(4 + \frac{\pi^2}{2}\right)\cdot\sqrt{\frac{E^2\pi R^6}{16(m - \rho V)g\rho_s L^4}}\right]. \quad (5)$$

Here, m and V are the mass and volume of the suspended sinker, L and E are the length and Young's modulus of the wire, g is the gravitational acceleration, and A is an empirical constant close to unity included to allow for deviations from the idealized end-clamped conditions. In equation (5), the first and dominant term is associated with tension as the restoring force, while the second is associated with stiffness and the third is a cross term. Under typical conditions, these terms comprise about 95 %, 4.5 % and 0.5 % of the observed resonance frequency

The instrument can be operated in either relative or absolute mode. In the relative mode of operation, a fluid of known viscosity and density is required to calibrate the radius of the wire and the volume of the suspended sinker. In the absolute mode, these and other physical parameters are obtained by direct measurement. In the present work, both modes of operation were used: relative mode was used for (CO_2 + $C_{16}H_{34}$) in the first campaign of measurements; absolute mode was used for (CH_4 + $C_{16}H_{34}$) in the second campaign; and pure $C_{16}H_{34}$ was studied by both methods. The properties of the wire and sinker are discussed in detail below.

The vibrating wire assembly was housed inside a pressure vessel, as illustrated in Figure 1, with a maximum working pressure of 200 MPa at T = 473.15 K. The pressure vessel was in turn housed within an insulated aluminum block, the temperature of which was regulated in three zones by means of process controllers each operating with a platinum resistance thermometer (PRT) and a set of electric cartridge heaters embedded in the aluminum block. This arrangement provided temperature stability within ±0.02 K and uniformity within ±0.1 K.

The temperature of the fluid was inferred from the reading of a PRT inserted into a thermowell

bored in the cap of the pressure vessel. This thermometer was calibrated at the temperature of the triple-point of water and, by comparison in an oil bath with a standard platinum resistance thermometer (SPRT), at temperatures from (313 to 433) K. The SPRT used had been calibrated previously on ITS-90 at the UK National Physical Laboratory. The standard uncertainty of the temperature measurement at the thermowell was estimated to be 0.01 K. However, to account for temperature gradients across the pressure vessel, the overall standard uncertainty ascribed to the temperature was 0.1 K.

During the measurements on (CO_2 + $C_{16}H_{34}$), the pressure was measured with a resonant quartz-crystal transducer (Paroscientific Inc., model 430K-101) whereas, during the measurements on (CH_4 + $C_{16}H_{34}$), the pressure was measured with a strain-gauge transducer (Stellar Technology Inc., model GT1600). Both transducers were calibrated over their full working ranges of (0 to 207) MPa against of a hydraulic dead-weight tester (DH Budenberg, model 580 EHX). During calibration, the combined effects of non-linearity, hysteresis and zero drift were found to be no worse than ±0.02 MPa. Considering also the specifications provided by the manufacturer, we take the overall standard uncertainty to be 0.02 MPa for measurements performed with the resonant quartz-crystal transducer and 0.2 MPa for the measurements performed with the strain-gauge transducer.

The pressure vessel was equipped with fluid ports at both top and bottom. These ports were connected via 6.35 mm o.d. high-pressure tubing to the two ports of a fluid-handling system as shown in Figure 2. The latter comprised a pressure generator, circulating pump, pressure transducer and valves. Operation of the circulation pump allowed the fluid to flow through the pressures vessel and around a circuit connecting the other devices, and this served to homogenize mixtures after sequential injection of the components. The pressure generator (Sitec-Sieber Engineering AG, model 750.1200) had a swept volume of 15 cm^3 and could rise pressure to 100 MPa within two strokes. In order to handle the mixtures at pressures above their bubble point, a medium pressure accumulator (PulseGuard Ltd, Model PiG-SS) was incorporated in parallel with the main circuit. This unit employed a gas-pressurized neoprene bladder as a variable-volume device and permitted up to 0.1 dm^3 of the mixture to be stored at pressures of up to 28 MPa. Valves permitted the accumulator to be either isolated from or incorporated within the flow loop so that it was possible to transfer mixture at $p \leq 28$ MPa to the pressure generator and then, after isolating the accumulator, to compress the sample to a higher pressure. The fluid handling system was located within a heated enclosure where the temperature could be regulated at up to 323 K and all interconnecting tubing was provided with electric trace heating. This permitted liquids such as hexadecane to be handled at high pressures without freezing.

To reduce the risk of fire or explosion in the event of leakage, the apparatus was installed in a well-ventilated laboratory fitted with flammable-gas alarms, and a nitrogen purge was used to obtain a non-oxidizing atmosphere within the fluid-handling system.

2.3 Vibrating-wire and sinker properties

For the absolute mode of operation, the wire radius R_0 at a reference temperature T_0 = 298.15 K and reference pressure p_0 = 0.1 MPa was obtained from measurements with a

laser micrometer (Aeroel SRL, model XLS13XY). The diameter was measured at three different points along the length of the wire and also in three different planes perpendicular to the axis of the wire, separated by 45°. The standard deviation of these measurements was 0.07 μm. The length L_0 of the assembled wire at the reference temperature and pressure was measured with a standard uncertainty of 0.01 mm by means of a precision internal caliper (Kroeplin, model H260) calibrated against a 70 mm i.d. setting ring. The radius and length of the wire at other temperatures and pressures were calculated from the relations

$$\left.\begin{aligned} \ln(R/R_0) &= \alpha_w(T-T_0) - \tfrac{1}{3}\beta_w(p-p_0) \\ \ln(L/L_0) &= \alpha_w(T-T_0) - \tfrac{1}{3}\beta_w(p-p_0) \end{aligned}\right\}, \tag{6}$$

where α_w is the linear thermal expansion coefficient and β_w is the isothermal compressibility of the wire, which were taken from the literature and assumed to be independent of T and p.

The volume V_0 of the sinker at the reference temperature and pressure was determined by hydrostatic weighing such that

$$V_0 = m\left[(I_{air}/I_{water})(\rho_{water}-\rho_{air})+\rho_{air}\right]^{-1}, \tag{7}$$

where m is the true mass of the sinker, and I_{air} and I_{water} are the apparent masses measured in air (of density ρ_{air}) and water (of density ρ_{water}), respectively.[44] All weighings were carried out on a precision electronic balance (Mettler Toledo, model PR5003) with a standard uncertainty of 5 mg. Values of the sinker volume at other temperatures and pressures were calculated from the relation

$$\ln(V/V_0) = 3\alpha_s(T-T_0) - \beta_s(p-p_0)\,, \tag{8}$$

where α_s is the linear thermal expansion coefficient and β_s is the isothermal compressibility of the sinker, which were taken from the literature and assumed to be independent of T and p.

The density $\rho_{w,0}$ of the wire material at $T = T_0$ was taken to be 19251 kg·m^{-3}, based on x-ray diffraction data from multiple laboratories as reported and analyzed by Parrish.[45] The wire density at other temperatures and pressures was calculated from

$$\ln(\rho_w/\rho_{0,w}) = -3\alpha_w(T-T_0) + \beta_w(p-p_0)\,. \tag{9}$$

Young's modulus of the wire material was expressed as a function of temperature (only) by means of the relation

$$\ln(E/E_0) = \varepsilon_w(T-T_0)\,, \tag{10}$$

where $E_0 = E(T_0)$ and ε_w is a temperature coefficient assumed to be constant. E_0 and ε_w were obtained from a careful review and analysis of the available literature data on the elastic constants of tungsten.[46-52] It was observed that the values of Young's modulus reported in the literature varied somewhat depending upon whether the sample was monocrystalline or polycrystalline. Values of E_0/GPa^{-1} for monocrystalline samples of 409.8, 409.4, and 409.1 were reported by Featherston and Neighbours,[48], Bolef and de Klerk,[47] and Armstrong and Brown,[50] respectively, while values of 401.7, 403.3, 402.7, and 395 were reported for polycrystalline samples by Lowrie and Gonas,[49] Bernstein,[46] Armstrong and Brown,[50] and Harrigill and Krsek.[51] Figure 3 shows values of E/E_0 for both mono- and poly-crystalline tungsten as a function of temperature. The data at $T \geq T_0$ conform to equation (10) and the value of ε_w,

based on an unweighted fit to all of the data at $T \geq T_0$, was found to be 9.7 x 10^{-5} K^{-1}.

The values, source and uncertainties of the coefficients α_w, α_s, β_w, β_s and ε_w are detailed in Table 5. The uncertainties were estimated based on the variability of the literature data.[45-49, 53, 54]

The empirical constant A and the vacuum decrement Δ_0 can be obtained in principle from a measurement of the resonance frequency and bandwidth of the oscillator in vacuum. However, since it is difficult to obtain a good vacuum in a high-pressure vessel when pumping through small-bore tubing, A and Δ_0 were instead inferred form measurements carried out in air or nitrogen at ambient pressure and T = 298.15 K. In this case, β and β' were calculated from the known properties of the gas at the temperature in pressure in question. In view of the reported differences between the value of Young's modulus discussed above, we adjusted the value of E_0 so as to obtain an optimal representation of the vacuum resonance frequency over the full temperature range of operation. The value obtained varied slightly from one wire sample to another but was typically 390 GPa^{-1} which is about 10 GPa^{-1} lower than the mean of the literature values for polycrystalline tungsten. Accordingly, we ascribe a standard uncertainty of of 10 GPa^{-1} to the value of E_0.

In the relative mode of operation, the radius R_0 of the wire and the volume V_0 of the sinker at the reference temperature and pressure were obtained by calibration with octane. The viscosity of octane under those conditions was taken to be η = (0.5092 ± 0.0015) mPa·s, as recommended by Dymond and Øye,[55] while the density was taken to be 698.3 $kg \cdot m^{-3}$ from the equation of state of Span and Wagner.[56] In this case, the length L_0 of the assembled wire at the reference temperature and the pressure was measured with a digital cathetometer with a standard uncertainty of 0.025 mm.

2.4 Measurement procedure

Prior to the commencement of any measurement cycle, the system was flushed with hexane, drained and dried under vacuum. Hexadecane was transferred to a glass reservoir, fitted with a dip tube for liquid withdrawal, and degassed under vacuum with stirring for about 30 minutes. The liquid was then drawn into the previously evacuated fluid-handling system.

Mixtures were prepared *in-situ*. The amount of liquid introduced was determined by weighing the sample bottle and its contents before and after the transfer, with liquid in the transfer tube allowed to drain back into the reservoir before the second weighing. The second component (CO_2 or CH_4) was transferred from the original supply cylinder to a 500 mL high-pressure stainless steel sample cylinder. In the case of CH_4, a compressor was used to raise the filing pressure to about 30 MPa. The sample cylinder was then connected to the fluid-handling system through the port previously used to introduce the liquid and the second component was then admitted to the system, thereby pushing the liquid remaining in the dead-volume of the inlet port fully into the system. The addition of the second component was monitored by continuous weighing of the sample cylinder, but the precise amount was determined from careful weighing of the uncoupled cylinder before and after the transfer. The amount lost in the dead volume between the cylinder and the inlet valve was determined by means of additional weighing operations. Use of the accumulator provided sufficient volume variation

for measurements to be carried out from just above the bubble pressure to approximately 100 MPa without the need to refill the system.

After injection of the required amount of liquid and gas into the system, the pressure of the system was raised to slightly above the bubble pressure at the temperature of the fluid handling system (typically 313 K). The circulation pump was then actuated and allowed to run continuously for 7 to 10 hours to homogenize the mixture. During this time, the system pressure was monitored to observed to approach a steady value. During measurements, the circulation pump was stopped and the pressure was adjusted to the desired value by means of the pressure generator. Measurements were made along isotherms, starting at the lowest pressure, proceeding to the highest pressure in roughly even increments and finally returning to the initial pressure for a check measurement. For pure hexadecane, the maximum pressure was restricted by freezing at either the measurement temperature or the temperature of the fluid handling system, which ever was lower. Since the solid-liquid phase diagram of the mixtures was unknown, roughly the same pressure limits were applied for the mixtures.

2.5 Validation measurement

Validation measurements were made prior to the start of the second measurement campaign because it was at this time that the absolute mode of operation was implemented. The validation measurements were conducted on a liquid viscosity standard S20 (Paragon Scientific Ltd) at ambient pressure and temperatures of (298.15, 310.91, 313.25, 323.15, 353.24 and 373.26) K. For purposes of interpolation and comparison, the viscosity reference data provided by the supplier was represented by the equation

$$\eta = A_\eta \exp\left(\frac{B_\eta}{T + C_\eta}\right), \tag{11}$$

where A_η, B_η, and C_η are constants, while the density reference data were represented by a quadratic polynomial in T. Figures 4 and 5 compare our validation measurements of viscosity and density, and also the reference data provided by the manufacturer, with these correlations. The relative deviations of our measurements were generally within the overall experimental uncertainty of the measuring device which, as discussed below, is about 0.3 % for the density and 2 % for the viscosity of a single substance at 95 % confidence.

2.6 Uncertainty analysis

The overall standard relative uncertainties $u_\mathrm{r}(\rho)$ of density and $u_\mathrm{r}(\eta)$ of viscosity are calculated from the following relations:

$$u_\mathrm{r}^2(\rho) = \sum_i \left[(\partial \ln \rho / \partial \ln z_i)_{z_{j\neq i}} u_\mathrm{r}(z_i)\right]^2 , \tag{12}$$

and

$$u_\mathrm{r}^2(\eta) = \sum_i \left[(\partial \ln \eta / \partial \ln z_i)_{z_{j\neq i}} u_\mathrm{r}(z_i)\right]^2 , \tag{13}$$

where z_i (i = 1, 2, 3 ⋯) are the sets of quantities that serve to determine ρ and η. In this work, we have developed a fully-analytical treatment for all the differential coefficients $(\partial \ln \rho / \partial \ln z_i)_{z_{j\neq i}}$ and $(\partial \ln \eta / \partial \ln z_i)_{z_{j\neq i}}$ that appear in these relations in the case of a pure fluid. This treatment is detailed fully in the Supporting Information and involves considering f_{res} and $\Omega_{\mathrm{res}} = 2\pi f_{\mathrm{res}} \rho R^2 / \eta$ as the primary quantities fitted to experimental resonance curves. The standard uncertainties ascribed to these two quantities are based on the repeatability of the measurements. The overall uncertainty budgets for density and viscosity obtained in our analysis are summarised in Table 6 and 7, respectively, and include an estimate of systematic (type B) uncertainties which is based on the observed level of agreement in the validation measurements carried out on viscosity standard S20. For the density, the most important term is the repeatability of the vacuum resonance frequency and this is an area for improvement in future work. In the case of the viscosity, uncertainty terms associated with R, ρ, Ω_{res}, T and p are all important. The tabulated uncertainties pertain to the median state point and to the absolute mode of operation. However, values at other state points and in the relative mode of operation are quite similar and, overall, we ascribe fixed expanded relative uncertainties to all state points as follows: $U_{\mathrm{r}}(\rho)$ = 0.3 % and $U_{\mathrm{r}}(\eta)$ = 2 % at 95 % confidence.

In the case of the binary mixtures, additional terms corresponding to the uncertainty in the mole fraction x is included in the analysis. To facilitate this calculation, the derivatives $(\partial \ln \rho / \partial x)_{T,p}$ and $(\partial \ln \eta / \partial x)_{T,p}$ were estimated from the data at selected temperatures and pressures covering the full ranges investigated. The mole fraction uncertainty was evaluated from the uncertainties in the masses m_1 of either CO_2 or CH_4 and m_2 of $C_{16}H_{34}$. These uncertainties were estimated to be $u(m_1)$ = 0.03 g and $u(m_2)$ = 0.06 g based mainly on the uncertainty associated with dead volumes in the interconnecting tubing. The corresponding uncertainty in the mole faction x of the light component is given by

$$u(x) = x(1-x)\left[u_{\mathrm{r}}^2(m_1) + u_{\mathrm{r}}^2(m_2)\right]^{1/2}. \qquad (14)$$

In the example case of the mixture xCH$_4$ + (1 - x)C$_{16}$H$_{34}$ at x = 0.3979, the corresponding masses were m_1 = 6.145 g and m_2 = 131.26 g, leading to $u(x)$ = 0.0013. For this mixture, $\left|(\partial \ln \rho / \partial x)_{T,p}\right| \leq 0.03$ and $\left|(\partial \ln \eta / \partial x)_{T,p}\right| \leq 0.5$, so that the composition uncertainty alone corresponds to uncertainties of < 0.01 % in density and about 0.05 % in viscosity. Accordingly, the composition uncertainty does not significantly inflate the uncertainties estimated in the case of a pure substance.

3. EXPERIMENTAL RESULTS

The viscosity and density of pure hexadecane and its binary mixtures with dissolved carbon dioxide or methane were measured. For the pure hexadecane, measurements were conducted along eight isotherms over a temperature range between (298.15 to 473.15) K in steps of 25 K and at pressures from 0.1 MPa up to approximately (80 or 100) MPa, except at T = 298.15 K where the maximum pressure was about 30 MPa. Higher pressures were prevented by freezing of the sample in the fluid-handling system and/or the interconnecting tubing. Table 8a presents the experimental results for hexadecane measured in relative mode, whereas Table 8b presents the results obtained in absolute mode.

For $x CO_2 + (1 - x) C_{16}H_{34}$, measurements were made with x = (0.0690, 0.5877 and 0.7270) and the results are presented in Tables 9 to 11. For $x CH_4 + (1 - x) C_{16}H_{34}$, measurements were made with x = (0.1013, 0.2021, 0.2976 and 0.3979) and the results are presented in Tables 12 to 15. In both systems, measurements were made in the temperature range between (298.15 and 473.15) K and at pressures up to between (30 and 120) MPa. Figures 6a and 6b illustrate the experimental data for $x CH_4 + (1 - x) C_{16}H_{34}$ at a fixed mole fraction of 0.2021 as a function of pressure at different temperatures, while Figure 7a and 7b illustrate the experimental data for $x CO_2 + (1 - x) C_{16}H_{34}$ at a fixed temperature of 423.21 K as functions of pressure at various compositions.

4. DATA CORRELATIONS

4.1 Correlation of density and viscosity at constant composition

The density of both pure hexadecane and its binary mixtures with CH_4 or CO_2 have been correlated using the modified Tait equation:[57]

$$\rho / (\mathrm{kg \cdot m^{-3}}) = \rho_0 \left[1 - C \log \left(\frac{p + B}{p_0 + B} \right) \right]^{-1} . \tag{15}$$

Here, C is a constant, and ρ_0 is the reference density at p_0 = 0.1 MPa and was expressed as a quadratic function in temperature as follows:

$$\rho_0 / (\mathrm{kg \cdot m^{-3}}) = \sum_{i=0}^{2} a_i (T / T_0)^i , \tag{16}$$

where T_0 = 298.15 K. The parameter B in eq 15 was expressed as a quadratic function in temperature:

$$B / \mathrm{MPa} = \sum_{i=0}^{2} b_i (T / T_0)^i . \tag{17}$$

The viscosity data were correlated by means of the Tait-Andrade equation:[58]

$$\eta = A_\eta \exp \left(\frac{B_\eta}{T + C_\eta} \right) \left(\frac{p + E}{p_0 + E} \right)^D , \tag{18}$$

where D and E are functions of temperature as follows:

$$D = \sum_{i=0}^{2} d_i (T / T_0)^{-i} \tag{19}$$

$$E / \mathrm{MPa} = \sum_{i=0}^{2} e_i (T / T_0)^i \tag{20}$$

The coefficients of eqs 15 to 17 and 18 to 20 were adjusted for density and viscosity respectively in a nonlinear optimization that minimized the average absolute relative deviation, defined for a property X as follows:

$$\Delta_{\mathrm{AAD}} = \frac{1}{N}\sum_{i=1}^{N}\left(\frac{\left|X_i - X_{i,\mathrm{fit}}\right|}{X_i}\right) \tag{21}$$

In eq 21, N is the total number of data points, X_i is an experimental datum, and $X_{i,\mathrm{fit}}$ is calculated from the correlation at the same state point. We also computed the maximum absolute relative deviation ($\Delta_{\mathrm{MAD},X}$) and the relative bias defined as follows:

$$\Delta_{\mathrm{MAD}} = \mathrm{Max}\left(\frac{\left|X_i - X_{i,\mathrm{fit}}\right|}{X_i}\right), \tag{22}$$

$$\Delta_{\mathrm{Bias}} = \frac{1}{N}\sum_{i=1}^{N}\left(\frac{X_i - X_{i,\mathrm{fit}}}{X_i}\right). \tag{23}$$

The optimisation was carried out individually for each mixture composition and the resulting fitting parameters are given in Tables 16 and 17, for density, and Tables 18 and 19 for viscosity (the results for pure hexadecane are included in Tables 16 and 18).

The correlations for density and viscosity describe our data very well for both pure hexadecane and the two binary mixtures. The quality of the correlations is illustrated in Figures 8 and 9 for density and viscosity of pure hexadecane respectively. Similarly, Figures 10a and 10b and 11a and 11b are density and viscosity deviation plots for $x\mathrm{CH_4}$ + (1 - x)$\mathrm{C_{16}H_{34}}$ at x = 0.2976 and $x\mathrm{CO_2}$ + (1 - x)$\mathrm{C_{16}H_{34}}$ at x = 0.5877, respectively. It is evident from the deviation plots that the correlations described our data approximately to within their estimated uncertainties. The statistical parameters, summarized in Tables 16 to 19, indicate that this is typical of all mixture compositions.

4.2 Comparison with literature

Several datasets exist in the literature on the density and viscosity of the pure hexadecane. For convenience, only datasets containing results at p > 0.1 MPa were compared with our results. Figure 12 shows the comparison of literature density data of pure hexadecane with eq 15. It can be seen from the figure that most of the datasets, especially the low pressure datasets, are in agreement with our measurements. For instance, the datasets from Outcalt *et al*.[59] and Glaser *et al*.[60] agree with our results to within the estimated uncertainty of our correlation, eq. 15. The rest of the data are comparable with our results but present a positive bias in the range of (0.1 to 0.3)%.

Similarly, available literature data on the viscosity of pure hexadecane were compared with eq 18 as shown in Figure 13. Again our data are in agreement with most of the available literature.

5. VISCOSITY MODELLING

5.1 Extended hard-sphere model

The extended hard-sphere model[40] was used in an attempt to model the viscosity of pure hexadecane and its binary mixtures with both carbon dioxide or methane. In this model, a reduced excess viscosity $\Delta\eta^*$ is defined as follows:

$$\Delta\eta^* = \frac{16}{5}(2N_A)^{\frac{1}{3}}\left(\frac{\pi}{MRT}\right)^{\frac{1}{2}}\left(\frac{V_m}{V_0}\right)^{\frac{2}{3}}\left(\frac{\eta-\eta_0}{R_\eta}\right), \quad (24)$$

where N_A is Avogadro's constant, M is the molar mass, R is the universal gas constant, V_m is the molar volume, V_0 is the molar core volume, η_0 is the dilute-gas viscosity and R_η is the roughness factor. Eq. 24 satisfies the condition that the excess viscosity $\Delta\eta^* \to 0$ as $V_m \to \infty$. The model asserts that $\Delta\eta^*$ is a universal function of the reduced volume V_m/V_0, which Ciotta et al.[40] obtained in the following form from an analysis of a large body of experimental data:

$$\log(1+\Delta\eta^*) = \sum_{i=1}^{7} c_i \left(\frac{V_0}{V_m}\right)^i; \quad (25)$$

the coefficients c_i are reported in the original paper.[40] The roughness factor is taken as a constant for each pure substance, while the molar core volumes are typically weak functions of temperature. Assael et al.[61] obtained roughness factors and characteristic molar core volume of the normal alkanes from methane to dodecane by fitting large experimental viscosity datasets in the temperature range of (298 to 400) K. Ciotta et al.[1] obtained R_η and V_0 for pure CO_2 by fitting viscosity data calculated from the reference-quality correlation of Vesovic et al.[62] at temperatures between 303 K and 448 K and for pressures such that $V_m/V_0 \le 5$. The results were correlated as a quadratic function of temperature as follows:

$$V_0/(\mathrm{cm^3\cdot mol^{-1}}) = \sum_{i=0}^{2} g_i (T/\mathrm{K})^i. \quad (26)$$

In the present work, we use these two literature sources for pure methane and pure carbon dioxide, respectively. In the case of hexadecane, we obtained R_η and the parameters in eq 26 by fitting to the present experimental data; the resulting parameters are given in Table 20.

To apply this model to the binary mixtures, the roughness factor $R_{\eta,\mathrm{mix}}$ and the molar core volume $V_{0,\mathrm{mix}}$ were estimated from those of the pure components via mixing rules. Usually, simple linear mole-fraction-weighted averages are employed for symmetric mixtures as follows:[3]

$$R_{\eta,\mathrm{mix}} = xR_{\eta,1} + (1-x)R_{\eta,2} \quad (27)$$

and

$$V_{0,\mathrm{mix}} = xV_{0,1} + (1-x)V_{0,2}. \quad (28)$$

Here, $R_{\eta,i}$ and $V_{0,i}$ are the roughness factor and characteristic molar core volume of pure component i. However, for highly asymmetric mixtures these linear mixing rules do not give a satisfactory estimation of the mixture viscosity. Therefore, in this work, several alternative mixing rules for $V_{0,\mathrm{mix}}$ have been tested in the prediction of the viscosities of the two binary mixtures studied. Note however that we retained the simple linear mixing rule for $R_{\eta,\mathrm{mix}}$, given

by eq 27. Each method was assessed in terms of Δ_{AAD} and Δ_{MAD} and the values of these quantities are given in Table 21 and are compared graphically in Figures 14 and 15. Since the correlation for V_0 of methane is restricted to $T \leq 400$ K, we applied the same restriction to our comparisons with experimental data.

5.2 Conventional linear mixing rule

The deviations of the experimental data from the extended-hard-sphere model with the conventional mixing rule for $V_{0,mix}$ are illustrated in Figure 16. These deviations range from (-10 to +48) % and one can observed that there is a systematic increase in the deviations as the mole fraction x of the light component is increased in both mixtures. Nevertheless, it is important to note that this mixing rule was applied without any adjustable parameters, and therefore it is not surprising that it gives large deviations due to the highly asymmetric nature of the mixtures as observed by Ciotta *et.al.*[1] in the case of CO_2 + squalane mixtures.

5.3 Linear mixing rule with an exponent

Since the linear mixing rule does not perform very well, we explored the use of a system-dependent but mole-fraction independent exponent γ such that

$$V_{0,\mathrm{mix}}^{\gamma} = xV_{0,1}^{\gamma} + (1-x)V_{0,2}^{\gamma}. \tag{29}$$

In eq.29, γ was adjusted to minimise the sum of the squared relative differences between the experimental values and the correlations for each binary mixture; the resulting values are given in Table 22. It can be observed in Table 21 and Figure 17 that the introduction of one adjustable parameter improves the representation of the data except for small mole fractions of the light component. Nevertheless, some large deviations remain and it is interesting to note that the optimal value of γ is rather close to unity in both cases.

5.4 Simple quadratic mixing rule

Having attempted two forms of linear mixing rule and considering the small improvement observed when a fitting parameter was added, we consider a quadratic mixing rule as follows:

$$V_{0,\mathrm{mix}} = x^2V_{0,ii} + 2x(1-x)V_{0,ij} + (1-x)^2V_{0,jj}. \tag{30}$$

Here the terms $V_{0,ii}$ and $V_{0,jj}$ are the characteristic molar core volumes of components i and j in the mixture, which are identical to the core volumes of the pure species $V_{0,i}$ and $V_{0,j}$, while $V_{0,ij}$ is the unlike molar core volume which we obtained from an arithmetic-mean combining rule as follows:

$$V_{0,ij} = (1-l_{ij})\left(\frac{V_{0,i}+V_{0,j}}{2}\right). \tag{31}$$

Eq 31 includes an binary parameter l_{ij} which was adjusted to best fit the data for the two systems investigated; the results are given in Table 22. Table 21 and Figure 18 show that eq (30) performs about as well as eq (29) and again the largest deviations are found for small

mole fractions of the light component where the linear mixing rule performs better. In this case, the binary parameters are quite close to zero.

5.5 Quadratic mixing rule with exponent of one-third

An alternative quadratic mixing rule, based on molecular diameter rather than volume, is as follows:

$$V_{0,\mathrm{mix}}^{1/3} = x^2 V_{0,ii}^{1/3} + 2x(1-x)V_{0,ij}^{1/3} + (1-x)^2 V_{0,jj}^{1/3}, \tag{32}$$

where the unlike term is given by the combining rule

$$V_{0,ij}^{1/3} = (1-l'_{ij})\left(\frac{V_{0,i}^{1/3} + V_{0,j}^{1/3}}{2}\right), \tag{33}$$

with a new binary parameter l'_{12}. As shown in Figure 19, the results of fitting this model to the mixture data are generally very poor, especially for small mole fractions of the light component and in all mixtures containing CO_2. The binary parameters obtained are given in Table 22 and are not close to zero.

5.6 Quadratic mixing rule with exponent of two-third

The final quadratic mixing rule investigated was based on molecular cross-section as follows:

$$V_{0,\mathrm{mix}}^{2/3} = x^2 V_{0,ii}^{2/3} + 2x(1-x)V_{0,ij}^{2/3} + (1-x)^2 V_{0,jj}^{2/3}, \tag{34}$$

where the unlike term is given by

$$V_{0,ij}^{2/3} = (1-l''_{ij})\left(\frac{V_{0,i}^{2/3} + V_{0,j}^{2/3}}{2}\right), \tag{35}$$

and l''_{12} is an adjustable binary parameter the values of which are given in Table 22. Although this rule performs better than eq (32), Figure 20 shows that the results are still relatively poor. We remark that allowing any of the parameters γ, l_{12}, l'_{12} or l''_{12} to vary with temperature did not result in a significant improvement.

5.7 $V_{0,\mathrm{mix}}$ as an adjustable parameter

In this approach, the parameters for eq (26), for $V_{0,\mathrm{mix}}$ as a function of T, were optimized for each mixture composition separately and the resulting values are given in Tables 23 and 24. As indicated in Table 21 and in Figure 21, this approach mostly provides a good fit of the experimental data but the method is then a composition-specific correlation with less predictive capability. Interpolation could be used to obtain the parameters of eq (26) at intermediate compositions.

SUMMARY AND CONCLUSIONS

We have measured the viscosity and density of the binary mixtures of CH_4 or CO_2 with $C_{16}H_{34}$ using a vibrating wire apparatus operating over wide ranges of temperature, pressure and

composition, and in both absolute and relative modes. Correlations based on the modified Tait equation were developed for the density of pure $C_{16}H_{34}$ and each individual mixture with relative uncertainties within the expanded uncertainty of the measurement. Similarly, empirical correlations based on the Tait-Andrade equation were developed for the viscosities of pure $C_{16}H_{34}$ and each individual mixture with relative uncertainties again comparable to the uncertainty of the measurements. We have explored the ability of the extended-hard-sphere model to correlate and predict the viscosity under various assumptions relating to the molar core volumes. The simple linear mixing rule for $V_{0,mix}$ performed poorly, except at small mole fractions of the light component. The inclusion of a single adjustable parameter in either eq (29) or eq (31) was found to make a large improvement, except at small mole fractions of the light component. However, such models do not represent the data to within their uncertainty. Finally, when each mixture composition is fitted separately, the model is able to correlate most of the data to within ±5 %.

Supporting Information

The Supporting Information file provides a detailed analytical analysis of the uncertainties of density and viscosity when determined using the vibrating-wire instrument in the absolute mode of operation.

Funding

Malami Mohammed received a scholarship from the Federal Government of Nigeria under the "2010 NYSC President's Honours Award scheme" administered by the Petroleum Technology Development Fund.

References

(1) Ciotta, F.; Maitland, G.; Smietana, M.; Trusler, J. P. M.; Vesovic, V. Viscosity and Density of Carbon Dioxide + 2,6,10,15,19,23-Hexamethyltetracosane (Squalane). *J. Chem. Eng. Data* **2009**, *54*, 2436-2443.

(2) Ciotta, F.; Maitland, G.; Smietana, M.; Trusler, J. P. M.; Vesovic, V. Erratum: "Viscosity and Density of Carbon Dioxide + 2,6,10,15,19,23-Hexamethyltetracosane (Squalane)" [J. Chem. Eng. Data 2009, 54, 2436-2443]. *J. Chem. Eng. Data* **2010**, *55*, 4126-4126.

(3) Assael, M. J.; Dymond, J. H.; Papadaki, M.; Patterson, P. M. Correlation and Prediction of Dense Fluid Transport-Coefficients. 3. Normal-Alkane Mixtures. *Int. J. Thermophys.* **1992**, *13*, 659-669.

(4) Diller, D. E. Measurements of the Viscosity of Compressed Gaseous and Liquid Methane + Ethane Mixtures. *J. Chem. Eng. Data* **1984**, *29*, 215-221.

(5) Vargaftik, N. Dictionary of Thermophysical Properties of Gases and Liquids. *Corporate Source: MOSKVA* **1972**, 156-292.

(6) Abe, Y.; Kestin, J.; Khalifa, H. E.; Wakeham, W. A. The Viscosity and Diffusion Coefficients of the Mixtures of Four Light Hydrocarbon Gases. *Physica A* **1978**, *93*, 155-170.

(7) Giddings, J. G.; Kao, J. T. F.; Kobayashi, R. Development of a High-Pressure Capillary-Tube Viscometer and Its Application to Methane, Propane, and Their Mixtures in the Gaseous and Liquid Regions. *J. Chem. Phys.* **1966**, *45*, 578-586.

(8) Huang, E. T. S.; Swift, G. W.; Kurata, F. Viscosities and Densities of Methane-Propane Mixtures at Low Temperatures and High Pressures. *AIChE J.* **1967**, *13*, 846-850.

(9) Kestin, J.; Yata, J. Viscosity and Diffusion Coefficient of Six Binary Mixtures. *J. Chem. Phys.* **1968**, *49*, 4780-4791.

(10) Carmichael, L. T.; Berry, V. M.; Sage, B. H. Viscosity of a Mixture of Methane and Butane. *J. Chem. Eng. Data* **1967**, *12*, 44-47.

(11) Dolan, J. P.; Ellington, R. T.; Lee, A. L. Viscosity of Methane-n-Butane Mixtures. *J. Chem. Eng. Data* **1964**, *9*, 484-487.

(12) Diaz Pena, M.; Cheda, J. A. R. Viscosity of Alkane Mixtures. *An. Quim.* **1975**, *71*, 257 - 261.

(13) Bagzis, L. D. Viscosity of Saturated Hydrocarbon Mixtures. MSc Thesis, Oklahoma State University, 1969.

(14) Rabe, D. Experimental Determination of Dynamic Viscosity and Density of Binary Liquid Mixtures of n-Heptane with CO_2, CH_4, C_2H_6, C_3H_8 and of Toluene with CH_4 and C_3H_8. PhD Thesis, TU Berlin, Berlin, 1981.

(15) Volkov, O. I. K., V.S. Viscosity of Solutions of Methane in n-Octane and n-Decane on the Fluid-Vapour Equilibrium Line. *Ukr. khim. Zh. Russ.* **1974**, *40*, 88 - 90.

(16) Audonnet, F.; Padua, A. A. H. Viscosity and Density of Mixtures of Methane and n-Decane from 298 to 393 K and up to 75 MPa. *Fluid Phase Equilib.* **2004**, *216*, 235-244.

(17) Lee, A. L.; Eakin, B. E. Viscosity of Methane-n-Decane Mixtures. *J. Chem. Eng. Data* **1966**, *11*, 281-287.

(18) Daugé, P.; Baylaucq, A.; Marlin, L.; Boned, C. Development of an Isobaric Transfer Viscometer Operating up to 140 MPa. Application to a Methane + Decane System. *J. Chem. Eng. Data* **2001**, *46*, 823-830.

(19) Canet, X.; Baylaucq, A.; Boned, C. High-Pressure (up to 140 MPa) Dynamic Viscosity of the Methane+Decane System. *Int. J. Thermophys.* **2002**, *23*, 1469-1486.

(20) Gozalpour, F.; Danesh, A.; Todd, A. C.; Tohidi, B. Viscosity, Density, Interfacial Tension and Compositional Data for near Critical Mixtures of Methane + Butane and Methane + Decane Systems at 310.95 K. *Fluid Phase Equilib.* **2005**, *233*, 144-150.

(21) Peleties, F. Advanced Fluid Property Measurement for Oilfield Applications. PhD Thesis, Imperial College London, London, 2007.

(22) Daridon, J. L.; Cassiede, M.; Paillol, J. H.; Pauly, J. Viscosity Measurements of Liquids under Pressure by Using the Quartz Crystal Resonators. *Rev. Sci. Instrum.* **2011**, *82*, 095114-095114-11.

(23) Knapstad, B.; Skjølsvik, P. A.; Øye, H. A. Viscosity of the n-Decane-Methane System in the Liquid Phase. *Ber. Bunsen-Ges. Phys. Chem.* **1990**, *94*, 1156-1165.

(24) Nourozieh, H.; Kariznovi, M.; Abedi, J. Vapor–Liquid Equilibrium Measurement and Thermodynamic Modeling of Binary Systems (Methane + n-Tetradecane). *Fluid Phase Equilib.* **2012**, *318*, 96-101.
(25) Kestin, J.; Ro, S. T. The Viscosity of Nine Binary and Two Ternary Mixtures of Gases at Low Density. *Ber. Bunsen-Ges. Phys. Chem.* **1974**, *78*, 20-24.
(26) Jackson, W. M. Viscosities of the Binary Gas Mixtures, Methane-Carbon Dioxide and Ethylene-Argon. *J. Phys. Chem.* **1956**, *60*, 789-791.
(27) Abe, Y.; Kestin, J.; Khalifa, H. E.; Wakeham, W. A. The Viscosity and Diffusion Coefficients of the Mixtures of Light Hydrocarbons with Other Polyatomic Gases. *Ber. Bunsen-Ges. Phys. Chem.* **1979**, *83*, 271-276.
(28) Diller, D. E.; Van Poolen, L. J.; Dos Santos, F. V. Measurements of the Viscosities of Compressed Fluid and Liquid Carbon Dioxide+ Ethane Mixtures. *J. Chem. Eng. Data* **1988**, *33*, 460-464.
(29) Trautz, M. K., FTrautz,M.;Kurz,F The Friction, Heat Conduction and Diffusion in Gas Mixtures. XV. The Friction of Hydrogen, Nitrous Oxide, Carbon Dioxide and Propane, and Their Binary Mixtures. *Ann. Phys. Leipzig* **1931**, *8*, 981-1003.
(30) Barrufet, M. A.; Salem, S. K. E.-S.; Tantawy, M.; Iglesias-Silva, G. A. Liquid Viscosities of Carbon Dioxide + Hydrocarbons from 310 K to 403 K. *J. Chem. Eng. Data* **1996**, *41*, 436-439.
(31) Nourozieh, H.; Bayestehparvin, B.; Kariznovi, M.; Abedi, J. Equilibrium Properties of (Carbon Dioxide + n-Decane + n-Octadecane) Systems: Experiments and Thermodynamic Modeling. *J. Chem. Eng. Data* **2013**, *58*, 1236-1243.
(32) Nourozieh, H.; Kariznovi, M.; Abedi, J. Measurement and Correlation of Saturated Liquid Properties and Gas Solubility for Decane, Tetradecane and Their Binary Mixtures Saturated with Carbon Dioxide. *Fluid Phase Equilib.* **2013**, *337*, 246-254.
(33) Kariznovi, M.; Nourozieh, H.; Abedi, J. Phase Composition and Saturated Liquid Properties in Binary and Ternary Systems Containing Carbon Dioxide, n-Decane, and n-Tetradecane. *J. Chem. Thermodyn.* **2013**, *57*, 189-196.
(34) Cullick, A. S.; Mathis, M. L. Densities and Viscosities of Mixtures of Carbon Dioxide and n-Decane from 310 to 403 K and 7 to 30 MPa. *J. Chem. Eng. Data* **1984**, *29*, 393-396.
(35) Kariznovi, M.; Nourozieh, H.; Abedi, J. Experimental Results and Thermodynamic Investigation of Carbon Dioxide Solubility in Heavy Liquid Hydrocarbons and Corresponding Phase Properties. *Fluid Phase Equilib.* **2013**, *339*, 105-111.
(36) Chung, F. T. H.; Jones, R. A.; Nguyen, H. T. Measurements and Correlations of the Physical Properties of CO_2-Heavy Crude Oil Mixtures. **1988**.
(37) Hu, R.; Crawshaw, J. P.; Trusler, J. P. M.; Boek, E. S. Rheology of Diluted Heavy Crude Oil Saturated with Carbon Dioxide. *Energy Fuels* **2015**, *29*, 2785-2789.
(38) Simon, R.; Graue, D. J. Generalized Correlations for Predicting Solubility, Swelling and Viscosity Behavior of CO_2 -Crude Oil Systems. *J. Pet. Technol.* **1965**, *17*, 102-106.
(39) Emanuel, A. S., A Mixing Rule Method for Calculating the Viscosity of CO_2 and Low-Gravity Reservoir Oil. In *60th Annual Technical Conference and Exhibitionof the Society of Petroleum Engineers*, Society of Petroleum Engineers: Las Vegas, 1985; Vol. SPE 14229.
(40) Ciotta, F.; Trusler, J. P. M.; Vesovic, V. Extended Hard-Sphere Model for the Viscosity of Dense Fluids. *Fluid Phase Equilib.* **2014**, *363*, 239-247.
(41) Ciotta, F. Viscosity of Asymmetric Liquid Mixtures under Extreme Conditions. PhD Thesis, Imperial College London, London, 2010.
(42) Retsina, T.; Richardson, S. M.; Wakeham, W. A. The Theory of a Vibrating-Rod Viscometer. *Appl. Sci. Res.* **1987**, *43*, 325-346.
(43) Ciotta, F.; Trusler, J. P. M. Improved Understanding of Vibrating-Wire Viscometer-Densimeters. *J. Chem. Eng. Data* **2010**, *55*, 2195-2201.
(44) Moldover, M. R.; Trusler, J. P. M.; Edwards, T. J.; Mehl, J. B.; Davis, R. S. Measurement of the Universal Gas Constant R Using a Spherical Acoustic Resonator. *Phys. Rev. Lett.* **1988**, *60*, 249-252.
(45) Parrish, W. Results of the I.U.Cr. Precision Lattice-Parameter Project. *Acta Crystallogr.* **1960**, *13*, 838-850.
(46) Bernstein, B. T. Elastic Properties of Polycrystalline Tungsten at Elevated Temperatures. *J. Appl. Phys.* **1962**, *33*, 2140-2140.

(47) Bolef, D. I.; De Klerk, J. Elastic Constants of Single-Crystal Mo and W between 77° and 500°K. *J. Appl. Phys.* **1962**, *33*, 2311-2314.
(48) Featherston, F. H.; Neighbours, J. R. Elastic Constants of Tantalum, Tungsten, and Molybdenum. *Phys. Rev.* **1963**, *130*, 1324-1333.
(49) Lowrie, R.; Gonas, A. M. Dynamic Elastic Properties of Polycrystalline Tungsten, 24°–1800°C. *J. Appl. Phys.* **1965**, *36*, 2189-2192.
(50) Armstrong, P. E.; Brown, H. L. Dynamic Young's Modulus Measurements above 1000 °C on Some Pure Polycrystalline Metals and Commercial Graphites. *T. Metall. Soc. AIME* **1964**, *230*, 962-966.
(51) Harrigill, W. T.; Krsek, A., *Method for Measuring Static Young's Modulus of Tungsten to 1900 K*. National Aeronautics and Space Administration: Washington DC, 1972; Vol. TN-6794.
(52) Dodge, H. Young's Modulus of Drawn Tungsten and Its Variation with Change of Temperature, Including a Determination of the Coefficient of Expansion. *Phys. Rev.* **1918**, *11*, 311.
(53) Slack, G. A.; Bartram, S. F. Thermal-Expansion of Some Diamond-Like Crystals. *J. Appl. Phys.* **1975**, *46*, 89-98.
(54) Touloukian, Y. S.; Kirby, R. K.; Taylor, R. E.; Desai, P. D., *Thermal Expansion, Metalilic Elements and Alloys*. Plenum Publishing: New York, 1975; Vol. 12.
(55) Dymond, J. H.; Oye, H. A. Viscosity of Selected Liquid n-Alkanes. *J. Phys. Chem. Ref. Data* **1994**, *23*, 41-53.
(56) Span, R.; Wagner, W. Equations of State for Technical Applications. II. Results for Nonpolar Fluids. *Int. J. Thermophys.* **2003**, *24*, 41-109.
(57) Dymond, J. H.; Malhotra, R. The Tait Equation: 100 Years On. *Int. J. Thermophys.* **1988**, *9*, 941-951.
(58) Comunas, M. J. P.; Baylaucq, A.; Boned, C.; Fernandez, J. High-Pressure Measurements of the Viscosity and Density of Two Polyethers and Two Dialkyl Carbonates. *Int. J. Thermophys.* **2001**, *22*, 749-768.
(59) Outcalt, S.; Laesecke, A.; Fortin, T. J. Density and Speed of Sound Measurements of Hexadecane. *J. Chem. Thermodyn.* **2010**, *42*, 700-706.
(60) Glaser, M.; Peters, C. J.; Van Der Kool, H. J.; Lichtenthaler, R. N. Phase Equilibria of (Methane+n-Hexadecane) and (P, V_m, T) of n-Hexadecane. *J. Chem. Thermodyn.* **1985**, *17*, 803-815.
(61) Assael, M. J.; Dymond, J. H.; Papadaki, M.; Patterson, P. M. Correlation and Prediction of Dense Fluid Transport-Coefficients. 1. Normal-Alkanes. *Int. J. Thermophys.* **1992**, *13*, 269-281.
(62) Vesovic, V.; Wakeham, W. A.; Olchowy, G. A.; Sengers, J. V.; Watson, J. T. R.; Millat, J. The Transport-Properties of Carbon-Dioxide. *J. Phys. Chem. Ref. Data* **1990**, *19*, 763-808.
(63) Kariznovi, M.; Nourozieh, H.; Abedi, J. Measurement and Equation of State Prediction of Vapor–Liquid Equilibrium and Physical Properties for the System Methane + n-Octadecane. *Fluid Phase Equilib.* **2012**, *314*, 102-106.
(64) Dymond, J. H.; Young, K. J.; Isdale, J. D. Transport Properties of Nonelectrolyte Liquid Mixtures—II. Viscosity Coefficients for the n-Hexane + n-Hexadecane System at Temperatures from 25 to 100 C at Pressures up to the Freezing Pressure or 500 MPa. *Int. J. Thermophys.* **1980**, *1*, 345-373.
(65) Tanaka, Y.; Hosokawa, H.; Kubota, H.; Makita, T. Viscosity and Density of Binary Mixtures of Cyclohexane with n-Octane, n-Dodecane, and n-Hexadecane under High Pressures. *Int. J. Thermophys.* **1991**, *12*, 245-264.
(66) Matthews, M. A.; Rodden, J. B.; Akgerman, A. High-Temperature Diffusion, Viscosity, and Density Measurements in n-Hexadecane. *J. Chem. Eng. Data* **1987**, *32*, 317-319.
(67) Kuss, E., *pVT-Daten Bei Hohen Drücken: Mit 48 Tabellen*. Deutsche Gesellschaft für Mineralölwissenschaft und Kohlechemie: Hamburg, 1976; Vol. 4510.
(68) Amorim, J. A.; Chiavone-Filho, O.; Paredes, M. L. L.; Rajagopal, K. High-Pressure Density Measurements for the Binary System Cyclohexane + n-Hexadecane in the Temperature Range of (318.15 to 413.15) K. *J. Chem. Eng. Data* **2007**, *52*, 613-618.
(69) Banipal, T. S.; Garg, S. K.; Ahluwalia, J. C. Heat Capacities and Densities of Liquid n-Octane, n-Nonane, n-Decane, and n-Hexadecane at Temperatures from 318.15 K to 373.15 K and at Pressures up to 10 MPa. *J. Chem. Thermodyn.* **1991**, *23*, 923-931.

(70) Wu, Y.; Bamgbade, B.; Liu, K.; Mhugh, M. A.; Baled, H.; Enick, R. M.; Burgess, W. A.; Tapriyal, D.; Morreale, B. D. Experimental Measurements and Equation of State Modeling of Liquid Densities for Long-Chain n-Alkanes at Pressures to 265 MPa and Temperatures to 523 K. *Fluid Phase Equilib.* **2011**, *311*, 17-24.
(71) Chang, J.-S.; Lee, M.-J.; Lin, H.-M. Densities of Binary Mixtures of Hexadecane with m-Xylene and Tetralin from 333 K to 413 K and Pressures up to 30 MPa. *J. Chem. Eng. Data* **1998**, *43*, 233-237.
(72) Khasanshin, T. S.; Samuilov, V. S.; Shchemelev, A. P. Determination of the Thermodynamic Properties of Liquid n-Hexadecane from the Measurements of the Velocity of Sound. *J. Eng. Phys. Thermophys.* **2009**, *82*, 149-156.
(73) Ducoulombier, D.; Zhou, H.; Boned, C.; Peyrelasse, J.; Saintguirons, H.; Xans, P. Pressure (1-1000 Bars) and Temperature (20-100 °C) Dependence of the Viscosity of Liquid Hydrocarbons. *J. Phys. Chem.* **1986**, *90*, 1692-1700.
(74) Morávková, L.; Wagner, Z.; Linek, J. (P, V_m, T) Measurements of (Cyclohexane + Nonane) at Temperatures from 298.15 K to 328.15 K and at Pressures up to 40 MPa. *J. Chem. Thermodyn.* **2007**, *39*, 1637-1648.
(75) Baled, H. O.; Xing, D.; Katz, H.; Tapriyal, D.; Gamwo, I. K.; Soong, Y.; Bamgbade, B. A.; Wu, Y.; Liu, K.; McHugh, M. A.; Enick, R. M. Viscosity of n-Hexadecane, n-Octadecane and n-Eicosane at Pressures up to 243 MPa and Temperatures up to 534 K. *J. Chem. Thermodyn.* **2014**, *72*, 108-116.

Table 1. Literature data on the viscosity of methane + *n*-alkane and CO_2 + *n*-alkane mixtures at temperatures *T* and pressures *p*.

n-alkane	CH_4 + Alkane Systems			CO_2 + Alkane Systems		
	T /K	*p* /MPa	Reference	*T* /K	*p* /MPa	Reference
Methane	-	-	-	293 to 473	0.1 to 2.5	9, 25, 26
Ethane	100 to 523	0.1 to 35	4-6	210 to 468	0.1 to 37	27, 28
Propane	123 to 524	0.1 to 61	5-8	298 to 551	0.1	5, 27, 29
Butane	278 to 633	0.1 to 55	6, 9-11	298 to 468	0.1	27
Pentane	373	-	12	-	-	-
Hexane	256 to 373	0.6 to 8.2	12, 13	-	-	-
Heptane	185 to 373	1 to 11.8	12, 14	-	-	-
Octane	290 to 430	-	12, 15	-	-	-
Decane	276 to 431	0.6 to 140	13, 15-23	311 to 403	1.1 to 35	30-34
Tetradecane	294 to 448	-	24	323 to 373	0.9 to 6.0	32, 33
Octadecane	323 to 448	10	63	323 to 373	0.9 to 5.9	31, 35

Table 2. Literature data on the viscosity of CO_2 + crude oil mixtures at temperatures *T* and pressures *p*.

System	*T* /K	*p* /MPa	Ref.(s)
CO_2 + heavy crude	297 to 366	0.1 to 34.6	36
CO_2 + heavy crude	298	0.1 to 22	37
CO_2 + crude oil	316 to 366	2 to 16.4	38
CO_2 + crude oil	294 to 394	2 to 48	39

Table 3. Description of Chemical Samples. [a]

Chemical Name	Source	Purity as Supplied [b]	Estimated Purity	Analysis Method	Additional Purification
n-hexadecane	S. Aldrich	$w > 0.9900$	0.9983	GC-MS [c]	none
carbon dioxide	BOC	$x \geq 0.99995$	-	-	none
methane	BOC	$x \geq 0.99995$	-	-	none
octane	Fluka	$w \geq 0.995$	-	-	degassed
S20 Standard	Paragon	-	-	-	none

[a] Notation: w is mass fraction and x is mole fraction.
[b] Purities are as stated by the supplier except where an analysis method is specified.
[c] Gas chromatography-mass spectrometry

Table 4. Properties of the gas chromatography GC Column.

Analysis:	GC-MS
Technique:	Magnet EI + TIC
Column type:	BPX5: L = 30 m: d = 0.25 mm
Carrier gas:	Helium; G = 1 ml·min^{-1}
T ramp:	5 K·min^{-1} (from 333.15 to 593.15 K)
Hold time t:	1 min

Table 5. Properties z of the wire and sinker together with standard uncertainties $u(z)$ and standard relative uncertainties $u_r(z)$.

Dimensionless quantity z	z	$u(z)$	$10^2 u_r(z)$	Source
$\rho_{w,0}$/(kg·m^{-3})	19251.3	1.6	0.009	[45]
α_w/K^{-1}	4.5 x 10^{-6}	0.32 x 10^{-6}	7.0	[53]
β_w/MPa^{-1}	3.24 x 10^{-6}	0.03 x 10^{-6}	1.0	[46-49]
ε_w/K^{-1}	-9.7 x 10^{-5}	0.2 x 10^{-5}	5.0	This work
α_s/K^{-1}	23.6 x 10^{-6}	0.7 x 10^{-6}	3.0	[54]
β_s/MPa^{-1}	14.3 x 10^{-6}	0.7 x 10^{-6}	5.0	[54]

Table 6. Uncertainty Budget for the Density of Hexadecane at the Median State Point in Terms of Standard Uncertainty $u(z)$ and Standard Relative Uncertainty $u_r(z)$ of Dimensionless Parameter z and Arising Contribution $u_r(\rho)$ to the Overall Standard Relative Uncertainty of Density.

Dimensionless quantity z	z	$u(z)$	$10^2 u_r(z)$	$10^2 u_r(\rho)$
T/K	398.15	0.1	0.025	0.007
p/MPa	40.0	0.2	0.5	0.019
f_{res}/Hz	716.27	0.04	0.005	0.031
Ω_{res}	17.71	0.04	0.24	0.011
$f_{0,vac}$/Hz	850.6	0.2	0.023	0.142
m/kg	0.403 625	1.5×10^{-6}	0.0004	0.0003
V_0/cm^3	142.055	0.003	0.0021	0.002
R_0/μm	75.5	0.1	0.13	0.007
L_0/mm	66.13	0.01	0.015	0.002
E_0/GPa	390	10	2.6	0.001
ρ_s/(kg·m^{-3})	19264	50	0.26	0.031
α_w/K^{-1}	4.5×10^{-6}	0.32×10^{-6}	7	0.001
β_w/MPa^{-1}	3.24×10^{-6}	0.03×10^{-6}	1	0.000
ε_w/K^{-1}	-9.7×10^{-5}	0.5×10^{-5}	5	0.001
α_s/K^{-1}	23.6×10^{-6}	0.7×10^{-6}	3	0.019
β_s/MPa^{-1}	14.3×10^{-6}	0.7×10^{-6}	5	0.002
ρ/(kg·m^{-3})	734.5	0.44 [a]	0.06	0.06
Overall combined standard relative uncertainty				0.16

[a] Type B uncertainty.

Table 7. Uncertainty Budget for the Density of Hexadecane at the Median State Point in Terms of Standard Uncertainty $u(z)$ and Standard Relative Uncertainty $u_r(z)$ of Dimensionless Parameter z and Arising Contribution $u_r(\eta)$ to the Overall Standard Relative Uncertainty of Viscosity.

Dimensionless quantity z	z	$u(z)$	$10^2 u_r(z)$	$10^2 u_r(\eta)$
T/K	398.15	0.1	0.025	0.10
p/MPa	40.0	0.2	0.5	0.19
f_{res}/Hz	716.27	0.04	0.005	0.01
Ω_{res}	17.71	0.04	0.24	0.24
ρ/(kg·m^{-3})	734.5	1.2	0.16	0.33
R/μm	75.5	0.1	0.13	0.27
ρ_w/(kg·m^{-3})	19250	50	0.26	0.09
Δ_0	65 x 10^{-6}	20 x 10^{-6}	31	0.19
α_w/K^{-1}	4.5 x 10^{-6}	0.32 x 10^{-6}	7	0.01
β_w/MPa^{-1}	3.24 x 10^{-6}	0.03 x 10^{-6}	1	0.00
η/(mPa·s)	1.046	0.006 [a]	0.6	0.60
Overall combined standard relative uncertainty				0.8

[a] Type B uncertainty.

Table 8. Experimental Density ρ and Viscosity η of pure n-$C_{16}H_{34}$ at Temperatures T and Pressures p Obtained in the Relative or Absolute Mode of Operation.

p/MPa	ρ/(kg·m^{-3})	η/(mPa·s)	p/MPa	ρ/(kg·m^{-3})	η/(mPa·s)
(a) Relative Mode of Operation [a]					
	T = 298.36 K			T = 323.21 K	
1.08	769.2	3.109	1.25	751.7	1.872
10.01	775.0	3.497	21.10	765.2	2.387
21.09	781.2	4.032	40.99	776.9	2.957
30.50	786.4	4.534	60.49	787.1	3.598
1.06	769.2	3.107	80.32	796.0	4.381
			102.81	803.3	5.080
			1.09	751.5	1.874
	T = 348.20 K			T = 373.12 K	
1.01	734.4	1.255	1.24	717.3	0.910
20.05	749.2	1.570	20.08	733.9	1.136
40.52	762.5	1.939	40.70	748.6	1.397
60.68	773.7	2.356	60.76	760.8	1.678
80.45	783.5	2.806	80.76	771.3	1.988
100.94	791.9	3.278	100.22	780.9	2.303
1.07	734.5	1.251	1.21	717.3	0.911
	T = 398.21 K			T = 423.26 K	
1.23	700.1	0.693	1.42	682.4	0.544
20.45	719.1	0.872	20.79	704.2	0.691
40.75	735.1	1.066	40.90	721.5	0.845
60.56	748.2	1.265	60.04	735.2	0.998
80.39	759.4	1.488	80.49	747.7	1.171
100.46	769.4	1.710	100.02	758.2	1.348
1.67	700.4	0.694	1.36	682.2	0.542
	T = 448.23 K			T = 473.54 K	
1.17	664.1	0.438	1.25	645.4	0.359
20.22	688.7	0.559	20.77	674.2	0.469
40.50	708.1	0.689	40.98	695.3	0.579
60.46	723.5	0.820	60.77	711.8	0.688
80.43	736.5	0.958	80.50	725.5	0.803
100.27	748.0	1.098	101.08	738.1	0.924
1.10	664.0	0.437	1.27	645.8	0.360

p/MPa	ρ/(kg·m^{-3})	η/(mPa·s)	p/MPa	ρ/(kg·m^{-3})	η/(mPa·s)
(b) Absolute Mode of Operation [b]					
	T = 298.61 K			T = 323.22 K	
0.97	768.9	3.143	0.99	752.4	1.878
10.34	774.7	3.562	20.96	764.8	2.429
20.57	780.8	4.041	42.10	777.2	3.007
30.37	785.9	4.588	61.17	787.4	3.666
			81.17	796.0	4.471
	T = 348.20 K			T = 373.25 K	
0.61	734.8	1.275	1.37	717.7	0.926
20.37	749.8	1.595	19.85	733.7	1.148
40.78	762.9	1.970	40.19	748.6	1.399
62.00	773.9	2.398	59.97	760.4	1.692
80.38	783.3	2.813	81.31	771.4	1.995
	T = 398.28 K			T = 423.31 K	
1.05	700.3	0.697	1.46	682.9	0.554
21.19	719.6	0.879	20.61	704.4	0.699
41.29	735.3	1.082	40.76	721.8	0.853
59.99	747.8	1.267	60.12	735.2	1.012
80.67	759.3	1.498	80.99	748.2	1.189
	T = 448.48 K			T = 473.85 K	
1.23	663.8	0.445	1.40	645.2	0.367
20.75	688.9	0.571	21.26	674.3	0.478
40.68	707.8	0.702	41.04	694.7	0.590
60.65	723.1	0.831	61.19	711.3	0.706
80.72	736.2	0.970	81.71	725.7	0.815
99.65	747.8	1.102			

[a] Expanded uncertainties are $U(T)$ = 0.2 K, $U(p)$ = 0.04 MPa, $U(\rho)$ = 0.003ρ and $U(\eta)$ = 0.02η with a coverage factor k of 2.

[b] Expanded uncertainties are $U(T)$ = 0.20 K, $U(p)$ = 0.40 MPa, $U(\rho)$ = 0.003ρ and $U(\eta)$ = 0.02η with a coverage factor k of 2.

Table 9. Experimental Density ρ and Viscosity η of $x CO_2$ + (1 - x)$C_{16}H_{34}$ at Temperatures T, Pressures p, and Mole fraction x = 0.0690 Obtained in the Relative Mode of Operation.[a]

p/MPa	ρ/(kg·m^{-3})	η/(mPa·s)	p/MPa	ρ/(kg·m^{-3})	η/(mPa·s)
	T = 298.16 K			T = 323.15 K	
11.13	776.5	3.075	10.41	759.1	1.830
21.44	782.8	3.474	20.23	765.7	2.061
30.25	787.6	3.870	40.86	778.3	2.560
10.92	776.3	3.057	60.91	788.7	3.130
			80.84	798.2	3.755
	T = 373.08 K		99.87	806.0	4.474
10.38	726.3	0.927	10.42	759.2	1.827
21.47	735.9	1.048			
40.33	749.9	1.263		T = 423.11 K	
60.30	762.5	1.514	11.50	694.2	0.574
80.56	773.5	1.794	21.70	705.2	0.645
100.83	783.5	2.087	40.71	722.5	0.778
12.12	728.0	0.947	60.59	737.2	0.929
			80.74	750.0	1.083
			101.55	761.6	1.253
			11.89	694.7	0.576

[a] Expanded uncertainties are $U(T)$ = 0.20 K, $U(p)$ = 0.04 MPa, $U(x)$ = 0.0007, $U(\rho)$ = 0.003ρ and $U(\eta)$ = 0.02η with a coverage factor k of 2.

Table 10. Experimental Density ρ and Viscosity η of $x CO_2 + (1 - x) C_{16}H_{34}$ at Temperatures T, Pressures p, and Mole fraction x = 0.5877 Obtained in the Relative Mode of Operation.[a]

p/MPa	ρ/(kg·m^{-3})	η/(mPa·s)	p/MPa	ρ/(kg·m^{-3})	η/(mPa·s)
	T = 298.18 K			T = 323.15 K	
10.44	802.3	1.003	10.63	779.0	0.704
20.56	811.8	1.107	20.85	790.2	0.786
30.07	819.7	1.219	40.11	807.6	0.947
40.38	827.4	1.344	60.10	822.7	1.122
10.67	802.7	0.998	10.86	779.5	0.703
	T = 373.11 K			T = 423.11 K	
20.76	745.5	0.463	25.91	708.9	0.328
40.22	768.7	0.564	40.19	730.3	0.384
60.46	787.7	0.670	60.24	753.3	0.462
80.24	803.1	0.775	80.46	772.0	0.537
20.79	745.5	0.463	100.80	787.9	0.614
			118.17	799.8	0.683
	T = 473.15 K		25.97	709.4	0.330
43.72	697.7	0.292			
60.70	720.7	0.343			
80.45	742.0	0.402			
100.84	760.2	0.460			
120.61	775.2	0.520			
43.62	697.7	0.293			

[a] Expanded uncertainties are $U(T)$ = 0.20 K, $U(p)$ = 0.04 MPa, $U(x)$ = 0.0027, $U(\rho)$ = 0.003ρ and $U(\eta)$ = 0.02η with a coverage factor k of 2.

Table 11. Experimental Density ρ and Viscosity η of $x CO_2 + (1 - x)C_{16}H_{34}$ at Temperatures T, Pressures p, and Mole fraction x = 0.7270 Obtained in the Relative Mode of Operation.[a]

p/MPa	ρ/(kg·m^{-3})	η/(mPa·s)	p/MPa	ρ/(kg·m^{-3})	η/(mPa·s)
	T = 298.14 K			T = 323.12 K	
21.81	822.6	0.786	21.41	796.3	0.565
31.03	831.7	0.861	40.33	817.3	0.679
41.13	840.7	0.943	60.54	835.2	0.806
22.01	822.8	0.787	80.28	850.1	0.930
			100.23	863.2	1.064
	T = 373.08 K		119.92	874.7	1.204
26.60	752.7	0.365	21.23	796.3	0.565
40.83	773.0	0.424			
60.00	794.6	0.503		T = 423.11 K	
80.11	813.1	0.581	42.20	730.3	0.296
99.99	828.7	0.659	60.28	755.6	0.353
117.64	840.7	0.735	80.39	777.7	0.412
26.47	752.5	0.365	100.36	795.9	0.471
			120.21	811.4	0.529
	T = 473.26 K		42.08	730.1	0.296
61.33	719.1	0.268			
80.48	744.0	0.313			
100.59	765.1	0.360			
120.86	783.0	0.407			
61.09	718.9	0.267			

[a] Expanded uncertainties are $U(T)$ = 0.20 K, $U(p)$ = 0.04 MPa, $U(x)$ = 0.0022, $U(\rho)$ = 0.003ρ and $U(\eta)$ = 0.02η with a coverage factor k of 2.

Table 12. Experimental Density ρ and Viscosity η of $x CH_4 + (1 - x)C_{16}H_{34}$ at Temperatures T, Pressures p, and Mole fraction x = 0.1013 Obtained in the Absolute Mode of Operation.[a]

p/MPa	ρ/(kg·m^{-3})	η/(mPa·s)	p/MPa	ρ/(kg·m^{-3})	η/(mPa·s)
	T = 298.15 K			T = 323.22 K	
10.23	781.6	3.304	10.08	765.4	1.993
19.83	786.5	3.687	20.17	771.2	2.205
			40.02	783.4	2.690
	T = 373.26 K		60.00	793.2	3.255
10.00	732.3	0.967	78.56	801.7	3.927
20.17	740.6	1.112			
40.11	754.5	1.334		T = 423.31 K	
60.08	767.4	1.571	15.70	707.2	0.611
80.13	777.3	1.897	20.01	711.8	0.643
			40.03	728.0	0.816
	T = 473.17 K		60.02	740.7	1.004
40.03	705.1	0.591	80.07	754.2	1.133
60.04	721.8	0.687			
80.06	735.5	0.794			

[a] Expanded uncertainties are $U(T)$ = 0.20 K, $U(p)$ = 0.40 MPa, $U(x)$ = 0.0010, $U(\rho)$ = 0.003ρ and $U(\eta)$ = 0.02η with a coverage factor k of 2.

Table 13. Experimental Density ρ and Viscosity η of $x CH_4 + (1 - x)C_{16}H_{34}$ at Temperatures T, Pressures p, and Mole fraction x = 0.2021 Obtained in the Absolute Mode of Operation.[a]

p/MPa	ρ/(kg·m^{-3})	η/(mPa·s)	p/MPa	ρ/(kg·m^{-3})	η/(mPa·s)
	T = 298.22 K			T = 323.32 K	
10.04	775.4	3.308	10.01	756.6	1.901
19.95	781.3	3.742	20.10	763.2	2.147
			39.15	775.8	2.576
	T = 373.20 K				
10.05	721.1	0.926		T = 423.24 K	
12.61	723.4	0.951	10.31	686.8	0.557
20.02	729.5	1.037	10.87	687.6	0.556
40.26	744.4	1.270	20.03	697.4	0.625
60.35	757.1	1.521	40.04	715.6	0.762
65.05	759.8	1.586	60.08	730.3	0.912
			80.15	743.2	1.067
	T = 473.36 K		10.90	687.1	0.557
13.01	656.8	0.387			
20.07	666.6	0.425			
40.07	688.4	0.530			
60.04	706.1	0.627			
80.03	720.5	0.732			
12.98	656.9	0.388			

[a] Expanded uncertainties are $U(T)$ = 0.20 K, $U(p)$ = 0.40 MPa, $U(x)$ = 0.0018, $U(\rho)$ = 0.003ρ and $U(\eta)$ = 0.02η with a coverage factor k of 2.

Table 14. Experimental Density ρ and Viscosity η of $x CH_4 + (1 - x)C_{16}H_{34}$ at Temperatures T, Pressures p, and Mole fraction x = 0.2976 Obtained in the Absolute Mode of Operation.[a]

p/MPa	ρ/(kg·m^{-3})	η/(mPa·s)	p/MPa	ρ/(kg·m^{-3})	η/(mPa·s)
	T = 298.21 K				
20.07	780.7	3.712			
30.32	786.0	4.196			
	T = 373.41 K			T = 323.23 K	
24.10	738.2	1.038	20.40	769.6	2.151
40.14	749.9	1.222	21.74	770.3	2.146
60.03	762.2	1.465	40.22	781.5	2.597
80.10	773.7	1.749	60.04	791.5	3.162
24.09	738.5	1.040	79.91	800.3	3.859
			21.72	770.4	2.147
	T = 423.58 K				
20.55	703.3	0.606		T = 473.40 K	
22.75	705.4	0.618	24.48	676.6	0.431
40.09	720.8	0.734	40.13	693.5	0.501
60.24	735.9	0.873	60.11	710.7	0.600
80.36	748.5	1.030	79.93	724.7	0.717
20.51	703.1	0.612	24.50	676.6	0.427

[a] Expanded uncertainties are $U(T)$ = 0.20 K, $U(p)$ = 0.40 MPa, $U(x)$ = 0.0023, $U(\rho) = 0.003\rho$ and $U(\eta) = 0.02\eta$ with a coverage factor k of 2.

Table 15. Experimental Density ρ and Viscosity η of $x CH_4 + (1 - x)C_{16}H_{34}$ at Temperatures T, Pressures p, and Mole fraction x = 0.3979 Obtained in the Absolute Mode of Operation.[a]

p/MPa	ρ/(kg·m^{-3})	η/(mPa·s)	p/MPa	ρ/(kg·m^{-3})	η/(mPa·s)
	T = 298.33 K			T = 323.26 K	
13.91	781.1	3.321	14.53	763.7	1.887
20.03	784.6	3.548	14.75	763.9	1.918
30.04	791.0	3.938	20.04	766.5	2.058
			40.05	778.7	2.560
	T = 373.47 K				
16.68	730.1	0.921		T = 423.94 K	
16.74	729.9	0.942	16.53	696.8	0.565
20.01	732.4	0.970	16.61	697.1	0.555
40.02	747.6	1.170	20.03	700.1	0.587
54.72	756.7	1.365	40.01	718.3	0.717
56.03	757.3	1.364	56.15	730.8	0.822
	T = 473.68 K				
22.72	673.5	0.420			
25.73	676.9	0.435			
40.08	692.4	0.502			
60.00	709.8	0.596			
80.23	724.2	0.704			

[a] Expanded uncertainties are $U(T)$ = 0.20 K, $U(p)$ = 0.40 MPa, $U(x)$ = 0.0026, $U(\rho)$ = 0.003ρ and $U(\eta)$ = 0.02η with a coverage factor k of 2.

Table 16. Coefficients of Equations 15, 16 and 17 and Statistical Parameters for the Density Correlation of $xCO_2 + (1 - x)C_{16}H_{34}$ Mixtures at Different Compositions.

Coefficient	$x = 0.0$	$x = 0.0690$	$x = 0.5877$	$x = 0.7270$
C	1.986×10^{-1}	1.986×10^{-1}	1.986×10^{-1}	1.986×10^{-1}
a_0	9.530×10^{2}	9.669×10^{2}	9.239×10^{2}	8.337×10^{2}
a_1	-1.665×10^{2}	-1.852×10^{2}	2.026×10^{1}	2.496×10^{2}
a_2	-1.784×10^{1}	-1.215×10^{1}	-1.525×10^{2}	-2.882×10^{2}
b_0	3.896×10^{2}	4.356×10^{2}	3.410×10^{2}	3.115×10^{2}
b_1	-3.879×10^{2}	-4.730×10^{2}	-3.936×10^{2}	-3.804×10^{2}
b_2	1.016×10^{2}	1.373×10^{2}	1.150×10^{2}	1.168×10^{2}
$10^2\ \Delta_{AAD}$	0.03	0.02	0.04	0.08
$10^2\ \Delta_{MAD}$	0.21	0.04	0.11	0.14
$10^2\ \Delta_{Bias}$	-0.01	0.00	0.00	0.00

Table 17. Coefficients of Equations 15, 16 and 17 and Statistical Parameters for the Density Correlation of $xCH_4 + (1 - x)C_{16}H_{34}$ Mixtures at Different Compositions.

Coefficient	$x = 0.1013$	$x = 0.2021$	$x = 0.2976$	$x = 0.3979$
C	2.036×10^{-1}	2.036×10^{-1}	2.036×10^{-1}	2.036×10^{-1}
a_0	9.699×10^{2}	9.982×0^{2}	8.920×10^{2}	1.011×10^{3}
a_1	-1.907×10^{2}	-2.310×10^{2}	-6.040×10^{1}	-2.445×10^{2}
a_2	-4.460×10^{0}	1.646×10^{0}	-6.221×10^{1}	6.576×10^{0}
b_0	2.975×10^{2}	3.813×10^{2}	2.513×10^{2}	4.035×10^{2}
b_1	-2.421×10^{2}	-3.788×10^{2}	-1.800×10^{2}	-4.066×0^{2}
b_2	4.764×10^{1}	9.873×10^{1}	2.488×10^{1}	1.074×10^{2}
$10^2\ \Delta_{AAD}$	0.05	0.03	0.12	0.03
$10^2\ \Delta_{MAD}$	0.16	0.07	0.30	0.09
$10^2\ \Delta_{Bias}$	0.00	0.00	0.00	-0.01

Table 18. Coefficients of Equations 18, 19 and 20 and Statistical Parameters for the Viscosity Correlation of $x CO_2 + (1 - x) C_{16}H_{34}$ Mixtures at Different Compositions.

Coefficient	$x = 0$	$x = 0.0690$	$x = 0.5877$	$x = 0.7270$
A_η	2.693×10^{-2}	3.972×10^{-2}	1.105×10^{-2}	8.210×10^{-3}
B_η	1.006×10^{3}	7.986×10^{2}	1.245×10^{3}	1.311×10^{3}
C_η	-8.621×10^{1}	-1.083×10^{2}	-1.365×10^{1}	5.846×10^{0}
d_0	3.112×10^{0}	4.029×10^{1}	1.774×10^{0}	1.265×10^{0}
d_1	-7.475×10^{0}	-1.043×10^{2}	-2.127×10^{0}	-1.004×10^{0}
d_2	6.739×10^{0}	6.982×10^{1}	1.482×10^{0}	9.694×10^{-1}
e_0	7.346×10^{2}	5.793×10^{3}	2.691×10^{2}	2.939×10^{2}
e_1	-8.044×10^{2}	-8.527×10^{3}	-2.618×10^{2}	-2.755×10^{2}
e_2	2.441×10^{2}	3.190×10^{3}	8.140×10^{1}	7.914×10^{1}
$10^2\ \Delta_{AAD}$	0.8	0.3	0.2	0.3
$10^2\ \Delta_{MAD}$	2.6	0.8	0.7	1.0
$10^2\ \Delta_{Bias}$	0.0	0.0	0.0	0.0

Table 19. Coefficients of Equations 18, 19 and 20 and Statistical Parameters for the Viscosity Correlation of $x CH_4 + (1-x) C_{16}H_{34}$ Mixtures at Different Compositions.

Coefficient	$x = 0.1013$	$x = 0.2021$	$x = 0.2976$	$x = 0.3976$
A_η	2.887×10^{-2}	3.562×10^{-2}	3.119×10^{-2}	5.233×10^{-2}
B_η	9.544×10^{2}	7.926×10^{2}	9.043×10^{2}	6.305×10^{2}
C_η	-9.214×10^{1}	-1.182×10^{2}	-9.837×10^{1}	-1.404×10^{2}
d_0	-7.183×10^{0}	3.761×10^{0}	2.964×10^{2}	1.678×10^{5}
d_1	1.438×10^{1}	-5.856×10^{0}	-1.518×10^{2}	-2.414×10^{5}
d_2	-2.743×10^{0}	2.978×10^{0}	-1.492×10^{2}	6.555×10^{4}
e_0	1.633×10^{3}	2.132×10^{2}	-6.587×10^{4}	-1.115×10^{7}
e_1	-1.602×10^{3}	-2.698×10^{2}	8.963×10^{4}	1.120×10^{7}
e_2	3.788×10^{2}	1.215×10^{2}	-2.414×10^{4}	-7.812×10^{5}
$10^2\ \Delta_{AAD}$	1.1	0.8	0.6	0.8
$10^2\ \Delta_{MAD\eta}$	3.4	1.7	1.8	2.0
$10^2\ \Delta_{Bias}$	0.1	0.0	0.0	0.0

Table 20. Roughness Factors R_η, Parameters g_i in Equation (26) for the Molar Core Volume, and Statistical Parameters for the Viscosity of $C_{16}H_{34}$.

R_η	g_0	g_1	g_2	$10^2\,\Delta_{AAD}$	$10^2\,\Delta_{MAD}$	$10^2\,\Delta_{Bias}$
1.820	2.748×10^2	-2.312×10^{-1}	1.680×10^{-4}	2.5	5.2	2.1

Table 21. Average Absolute Relative Deviations Δ_{AAD} and Maximum Absolute Relative Deviation Δ_{MAD} of the Viscosity of Binary Mixtures From the Predictions of the Extended-Hard-Sphere Model With Different Equations for the Molar Core Volume $V_{0,mix}$.

Equation for $V_{0,mix}$	$x CH_4 + (1 - x)C_{16}H_{34}$				$x CO_2 + (1 - x)C_{16}H_3$		
	$x = 0.1013$	$x = 0.2021$	$x = 0.2976$	$x = 0.3979$	$x = 0.0690$	$x = 0.5877$	$x = 0.7270$
	$10^2\Delta_{AAD}$						
Eq. 28	3.8	20.6	27.0	38.5	2.1	10.4	29.3
Eq. 29	13.3	6.0	4.4	3.6	4.6	10.0	13.6
Eq. 30	12.7	6.3	4.3	3.3	5.6	9.7	15.9
Eq. 32	33.0	5.8	4.8	30.1	44.1	28.7	59.6
Eq. 34	19.8	2.8	4.8	11.2	20.9	8.7	33.4
Eq. 26	1.4	1.6	1.0	1.3	1.4	2.9	4.5
	$10^2\Delta_{MAD}$						
Eq. 28	9.7	25.8	40.9	47.5	7.8	14.4	31.3
Eq. 29	23.2	7.9	10.7	6.2	12.1	23.1	18.1
Eq. 30	22.4	8.2	11.1	6.0	13.5	22.5	19.5
Eq. 32	51.9	16.5	10.4	36.0	73.0	30.4	66.1
Eq. 34	32.6	7.2	10.4	13.8	36.5	20.9	35.4
Eq. 26	3.0	4.0	3.2	3.4	2.8	5.4	8.7

Table 22. Adjustable Parameters in Equations 29, 31, 33 and 35.

System	γ	l_{12}	l'_{12}	l''_{12}
$CH_4 + C_{16}H_{34}$	0.9649	0.0280	-0.2151	-0.1851
$CO_2 + C_{16}H_{34}$	1.0444	-0.0375	-0.2630	-0.2686

Table 23. Roughness Factors R_η, Parameters g_i in Equation (26) for the Molar Core Volume, and Statistical Parameters for the Viscosity of $x CH_4 + (1 - x)C_{16}H_{34}$.

Coefficient	x = 0.1013	x = 0.2021	x = 0.2976	x = 0.3976
R_η	1.737	1.654	1.576	1.494
g_0	3.002×10^2	2.627×10^2	3.159×10^2	1.767×10^2
g_1	-5.309×10^{-1}	-4.312×10^{-1}	-8.606×10^{-1}	-1.753×10^{-1}
g_2	6.328×10^{-4}	5.104×10^{-4}	1.134×10^{-3}	1.589×10^{-4}
$10^2\ \Delta_{AAD}$	1.4	1.6	1.1	1.3
$10^2\ \Delta_{MAD}$	3.0	4.0	3.2	3.4
$10^2\ \Delta_{Bias}$	0.2	0.2	0.1	0.1

Table 24. Roughness Factors R_η, Parameters g_i in Equation (26) for the Molar Core Volume, and Statistical Parameters for the Viscosity of $x CO_2 + (1 - x)C_{16}H_{34}$.

Coefficient	x = 0.0690	x = 0.5877	x = 0.7270
R_η	1.759	1.303	1.180
g_0	3.008×10^2	1.280×10^2	1.395×10^2
g_1	-4.770×10^{-1}	-1.137×10^{-1}	-3.439×10^{-1}
g_2	5.434×10^{-4}	1.063×10^{-4}	4.612×10^{-4}
$10^2\ \Delta_{AAD}$	1.4	2.9	4.5
$10^2\ \Delta_{MAD}$	2.8	5.4	8.7
$10^2\ \Delta_{Bias}$	0.2	0.5	1.1

Figures Captions:

Figure 1. Schematic of the vibrating-wire sensor assembly: (A) vibrating wire; (B) Sm-Co magnets; (C) sinker; (D) pressure vessel and (E) pressure vessel plug and screw cap.

Figure 2. Fluid-handling system: V-1, fluid inlet valve; V-2, vacuum valve; V-3 purge-gas inlet valve; V-4, drain valve; V-5, V-6, V-7, V-8, isolation valves; V-9, bypass valve; E-1, pressure generator; E-2 magnetic circulation pump; E-3, accumulator vessel; E-4, main pressure vessel; T-1, platinum resistance thermometer; P-1, pressure gauge; P-2, pressure transducer.

Figure 3. Ratio E/E_0 of Young's modulus E at temperature T to the corresponding value E_0 at T = 298.15 K. Empty symbols denote single crystalline and the filled symbols denote polycrystalline tungsten material. ○, Featherston and Neighbours;[48] □, Bolef and de Klerk; [47] ◇, Armstrong and Brown; [50] ▲, Lowrie and Gonas;[49] ■, Bernstein;[46] ◆, Armstrong and Brown;[50] ———**,** linear fit at $T \geq 200$ K.

Figure 4. (a) Density ρ and (b) relative density deviations $\Delta\rho/\rho$ of validation measurements and calibration data from a quadratic function of temperature T. ○, measurements; ■, calibration data.

Figure 5. (a) Viscosity η and (b) relative viscosity deviations $\Delta\eta/\eta$ of validation measurements and the calibration data from eq 11. as functions of temperature T. ○, measurements; ■, calibration data.

Figure 6. Experimental density ρ (a) and experimental viscosity η. (b) of $x CH_4 + (1 - x)C_{16}H_{34}$ at mole fraction x = 0.2021 as a function of pressure p at various temperatures T: ●, T = 298 K; □, T = 323 K; ◆, T = 373 K; △, T = 423 K; ∗, T = 473 K.

Figure 7. Experimental density ρ (a) and experimental viscosity η (b) of $CO_2 + (1 - x)C_{16}H_{34}$ at temperature T = 423.21 K as a function of pressure p at various CO_2 mole fractions x: ○, x = 0; ■, x = 0.0690; ◇, x = 0.5877; ▲, x = 0.7270.

Figure 8. Experimental density ρ (a) and fractional density deviations $\Delta\rho/\rho$ (b) for pure hexadecane as functions of pressure p at various temperatures: ◇, T = 298 K; □, T = 323 K; ○, T = 348 K △, T = 373 K; ×, T = 398 K; +, T = 423 K; –, T = 448 K; ∗, T = 473 K; ——, eq. 15. Red symbols are from relative-mode and blue symbols from absolute-mode measurements.

Figure 9. Experimental viscosity η (a) and fractional viscosity deviations $\Delta\eta/\eta$ (b) for pure hexadecane as functions of pressure p at various temperatures: ◇, T = 298 K; □, T = 323 K; ○, T = 348 K △, T = 373 K; ×, T = 398 K; +, T = 423 K; –, T = 448 K; ∗, T = 473 K; ——, eq. 18. Red symbols are from relative-mode and blue symbols from absolute-mode measurements.

Figure 10. Fractional deviations of density $\Delta\rho/\rho$ (a) and fractional deviations of viscosity $\Delta\eta/\eta$ (b) of $x CH_4 + (1 - x)C_{16}H_{34}$ at $x = 0.2976$ from the correlations, eqs. 15 and 18 as functions of pressure p: ◇, $T = 298$ K; □, $T = 323$ K; △, $T = 373$ K; +, $T = 423$ K; ∗, $T = 473$ K.

Figure 11. Fractional deviations of density $\Delta\rho/\rho$ (a) and fractional deviations of viscosity $\Delta\eta/\eta$ (b) of $x CO_2 + (1 - x)C_{16}H_{34}$ at $x = 0.5877$ from the correlations, eqs. 15 and 18 as functions of pressure p: ◇, $T = 298$ K; □, $T = 323$ K; △, $T = 373$ K; +, $T = 423$ K; ∗, $T = 473$ K.

Figure 12. Fractional deviations of density $\Delta\rho/\rho$ of pure hexadecane from eq. 15 as a function of pressure p: ●, This work relative mode; □, This Work absolute mode; ▲, Dymond *et al.*;[64] ×, Tanaka *et al.*;[65] ◇, Matthews *et al.*;[66] ○, Outcalt *et al.*;[59] _, Kuss;[67] +, Glaser *et al.*;[60] ∗, Amorim *et al.*;[68] △, Banipal *et al.*;[69] —, Wu *et al.*;[70] ■, Chang *et al.*;[71] ◆, Khasanshin *et al.*;[72] – – – –, relative uncertainty of eq. 15

Figure 13. Fractional deviations of viscosity $\Delta\eta/\eta$ of pure hexadecane from eq. 18 as a function of pressure p: ●, This work relative mode; □, This work absolute mode; ×, Ducoulombier *et al.*;[73]; ◇, Matthews *et al.*;[66] ▲, Rastorguev *et al.*;[74] ◆, Tanaka e*t al.*;[65] ■, Baled *et al.*;[75] ○, Dymond *et al.*;[64] – – – –, relative uncertainty of eq. 18.

Figure 14. Average absolute deviations of viscosity, $10^2\Delta_{AAD}$, from the hard-sphere model with different mixing rules: 1, conventional linear mixing rule for $V_{0,mix}$; 2, linear mixing rule for $V_{0,mix}^{\gamma}$; 3, quadratic mixing rule for $V_{0,mix}$; 4, quadratic mixing rule for $V_{0,mix}^{1/3}$; 4, quadratic mixing rule for $V_{0,mix}^{2/3}$; 6, $V_{0,mix}$ fitted to experimental data at each composition.

Figure 15. Maximum absolute deviations of viscosity, $10^2\Delta_{MAD}$, from the hard-sphere model with different mixing rules: 1, conventional linear mixing rule for $V_{0,mix}$; 2, linear mixing rule for $V_{0,mix}^{\gamma}$; 3, quadratic mixing rule for $V_{0,mix}$; 4, quadratic mixing rule for $V_{0,mix}^{1/3}$; 4, quadratic mixing rule for $V_{0,mix}^{2/3}$; 6, $V_{0,mix}$ fitted to experimental data at each composition.

Figure 16. Fractional deviation $\Delta\eta/\eta$ of experimental viscosity from the values estimated using eqs. 24 and 28. Blue empty symbols, $x CH_4 + (1 - x)C_{16}H_{34}$ with: □, $x = 0.1013$; ◇, $x = 0.2021$; △, $x = 0.2976$ and ○, $x = 0.3979$. Red symbols, $x CO_2 + (1 - x)C_{16}H_{34}$ with: ×, $x = 0.0690$; +, $x = 0.5877$ and ∗, $x = 0.7270$.

Figure 17. Fractional deviation $\Delta\eta/\eta$ of experimental viscosity from the values estimated using eqs. 24 and 29. Blue empty symbols, $x CH_4 + (1 - x)C_{16}H_{34}$ with: □, $x = 0.1013$; ◇, $x = 0.2021$; △, $x = 0.2976$ and ○, $x = 0.3979$. Red symbols, $x CO_2 + (1 - x)C_{16}H_{34}$ with: ×, $x = 0.0690$; +, $x = 0.5877$ and ∗, $x = 0.7270$.

Figure 18. Fractional deviation $\Delta\eta/\eta$ of experimental viscosity from the values estimated using eqs. 24, 30 and 31. Blue empty symbols, $x CH_4 + (1 - x)C_{16}H_{34}$ with: □, $x = 0.1013$; ◇, $x = 0.2021$; △, $x = 0.2976$ and ○, $x = 0.3979$. Red symbols, $x CO_2 + (1 - x)C_{16}H_{34}$ with: ×, $x = 0.0690$; +, $x = 0.5877$ and ∗, $x = 0.7270$.

Figure 19. Fractional deviation $\Delta\eta/\eta$ of experimental viscosity from the values estimated using eqs. 24, 32 and 33. Blue empty symbols, $x CH_4 + (1 - x)C_{16}H_{34}$ with: □, $x = 0.1013$; ◇, $x =$

0.2021; △, x = 0.2976 and ○, x = 0.3979. Red symbols, $x CO_2$ + (1 - x)$C_{16}H_{34}$ with: ×, x = 0.0690; ＋, x = 0.5877 and ∗, x = 0.7270.

Figure 20. Fractional deviation $\Delta\eta/\eta$ of experimental viscosity from the values estimated using eqs. 24, 34 and 35. Blue empty symbols, $x CH_4$ + (1 - x)$C_{16}H_{34}$ with: □, x = 0.1013; ◇, x = 0.2021; △, x = 0.2976 and ○, x = 0.3979. Red symbols, $x CO_2$ + (1 - x)$C_{16}H_{34}$ with: ×, x = 0.0690; ＋, x = 0.5877 and ∗, x = 0.7270.

Figure 21. Fractional deviation $\Delta\eta/\eta$ of experimental viscosity from the values estimated using eq 24 with V_0 fitted to eq 26 for each composition separately. Blue empty symbols, $x CH_4$ + (1 - x)$C_{16}H_{34}$ with: □, x = 0.1013; ◇, x = 0.2021; △, x = 0.2976 and ○, x = 0.3979. Red symbols, $x CO_2$ + (1 - x)$C_{16}H_{34}$ with: ×, x = 0.0690; ＋, x = 0.5877 and ∗, x = 0.7270.

Figure 1.

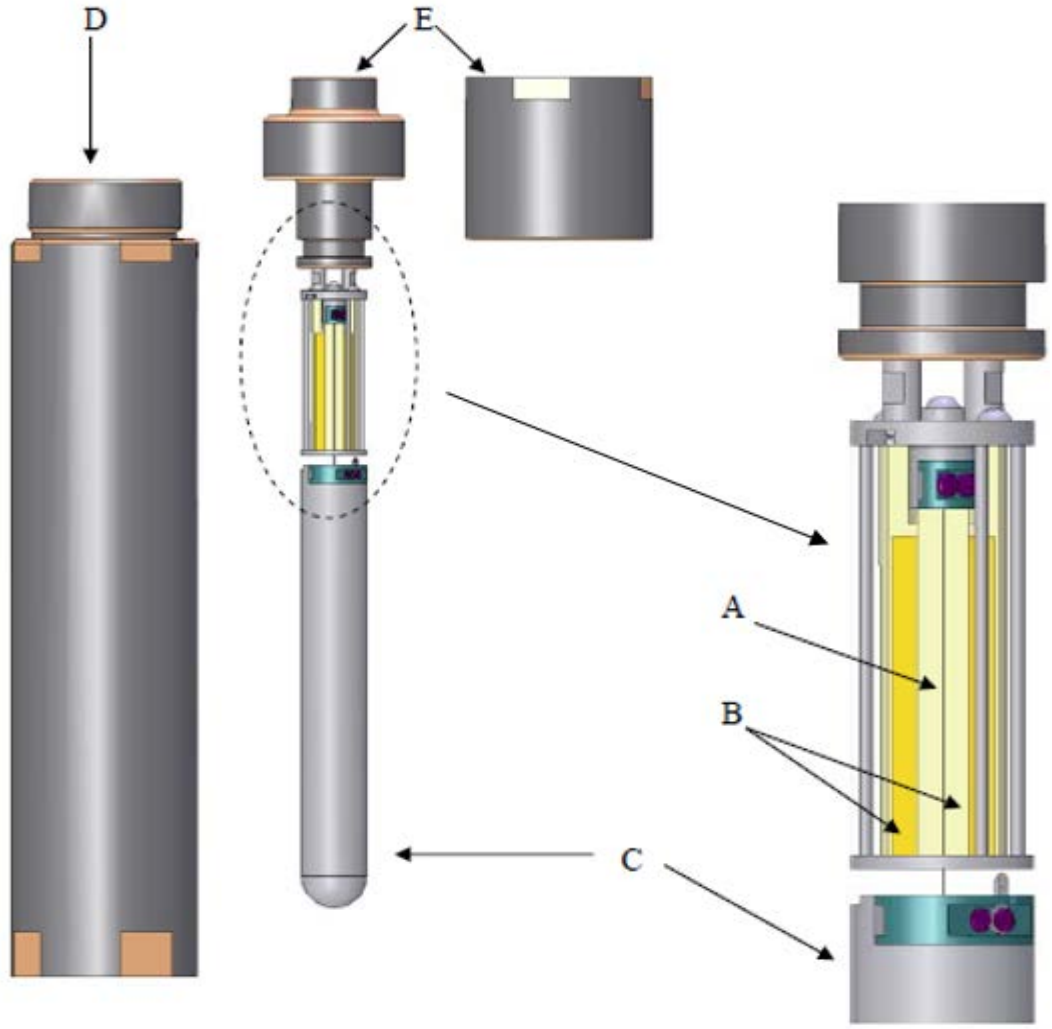

Figure 2.

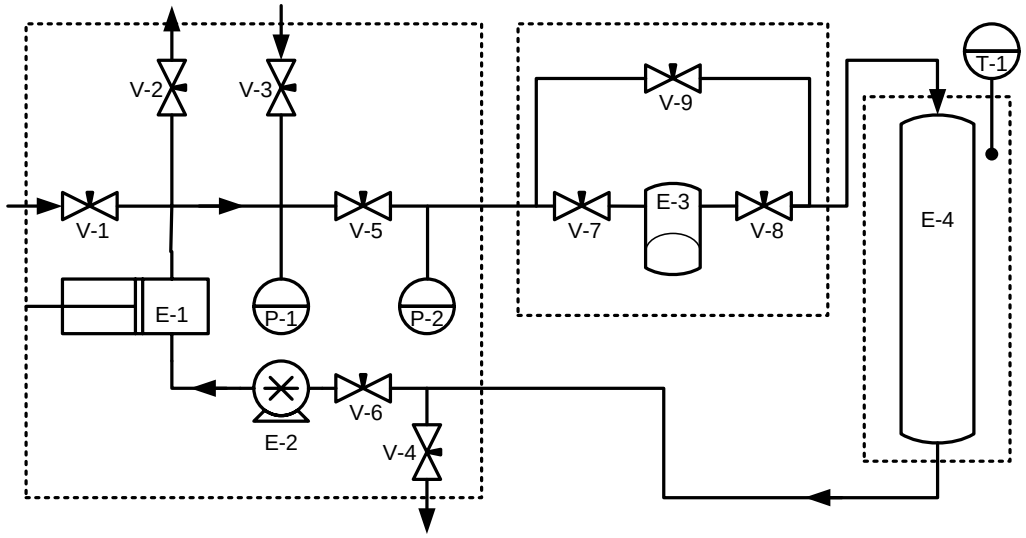

Figure 3.

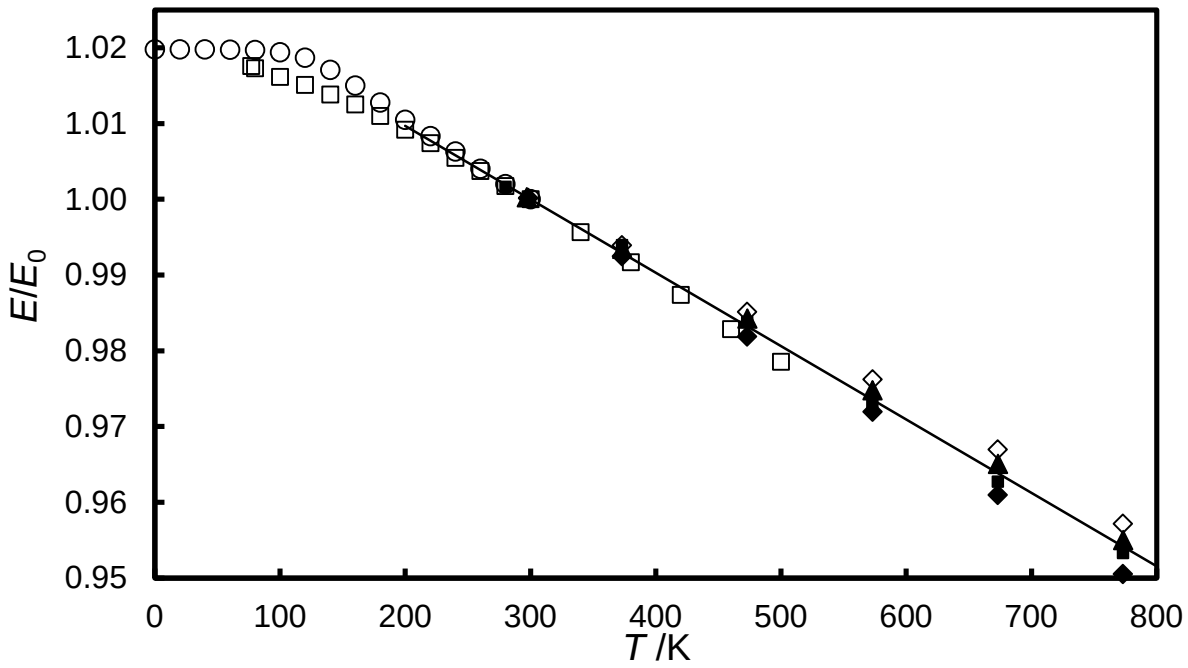
1.02
1.01
1.00
0.99
0.98
0.97
0.96
0.95
E/E0
0
100
200
300
400
500
600
700
800
T /K

Figure 4.

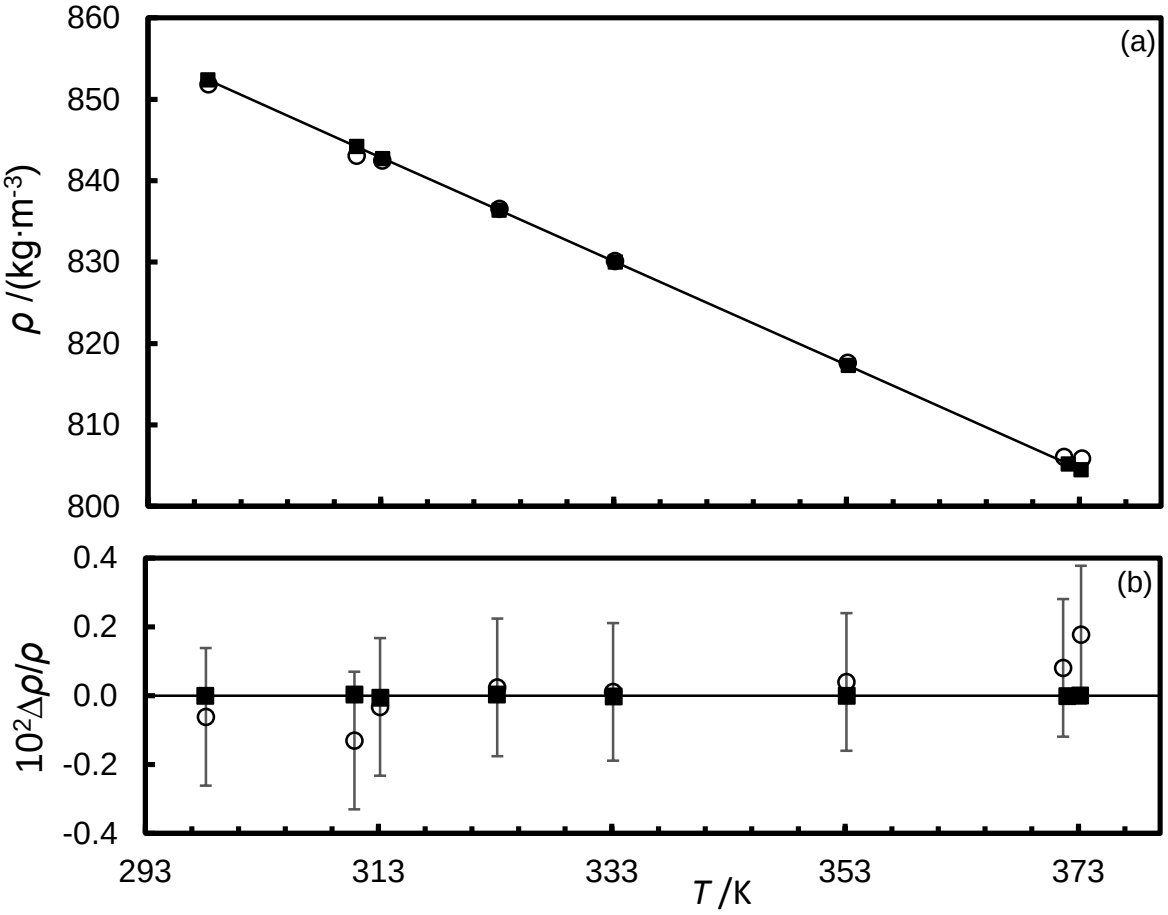
860
850
840
830
820
810
800
(a)
ρ /(kg·m-3)
0.4
0.2
0.0
-0.2
-0.4
(b)
10²Δρ/ρ
293
313
333
353
373
T /K

Figure 5.

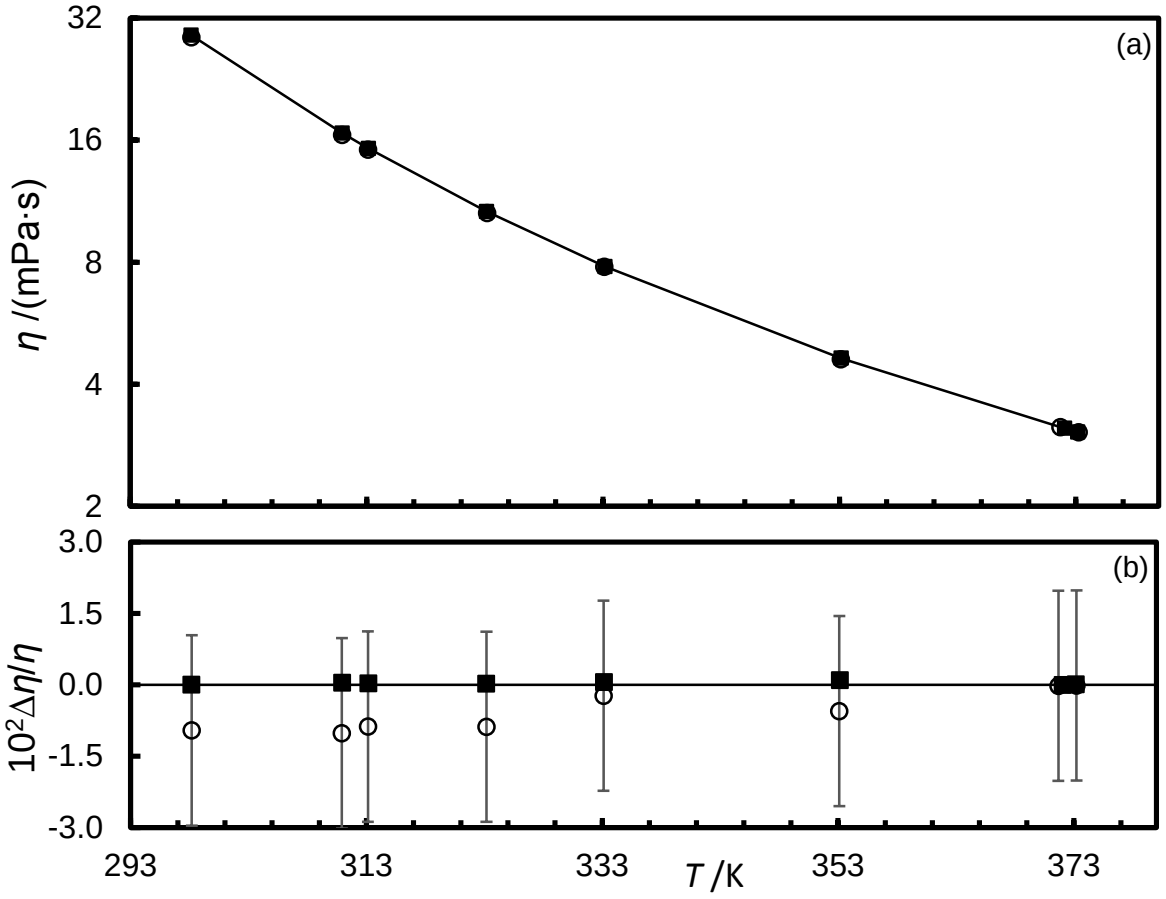

Figure 6.

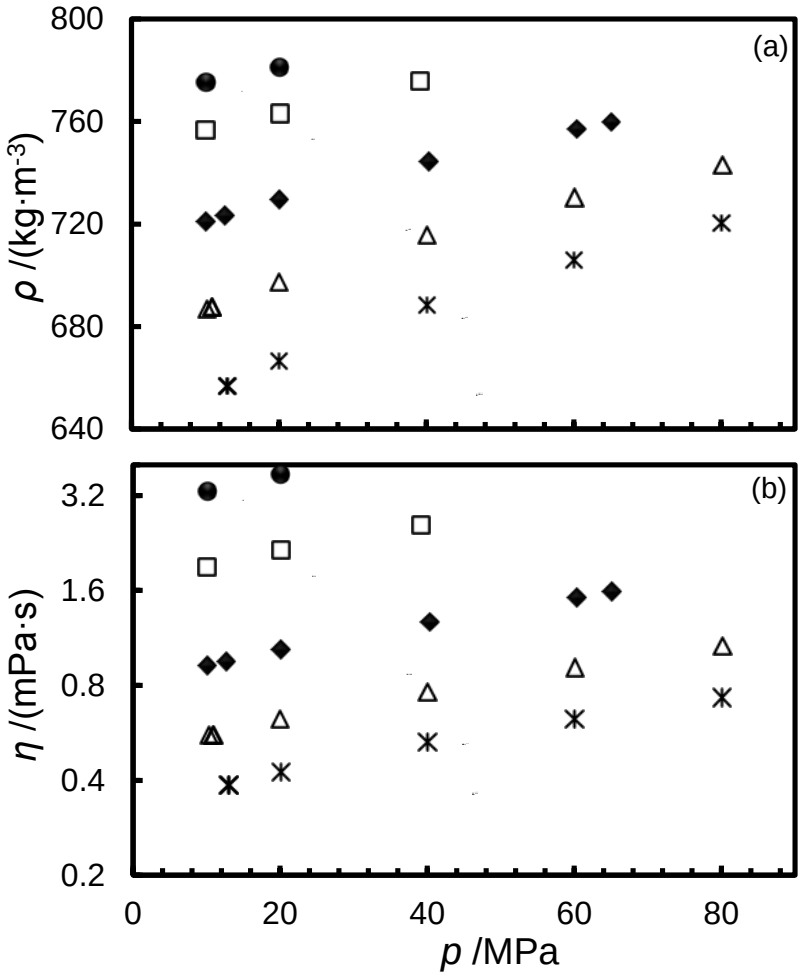
800
760
720
680
640
ρ /(kg·m-3)
(a)
3.2
1.6
0.8
0.4
0.2
η /(mPa·s)
(b)
0
20
40
60
80
p /MPa

Figure 7.

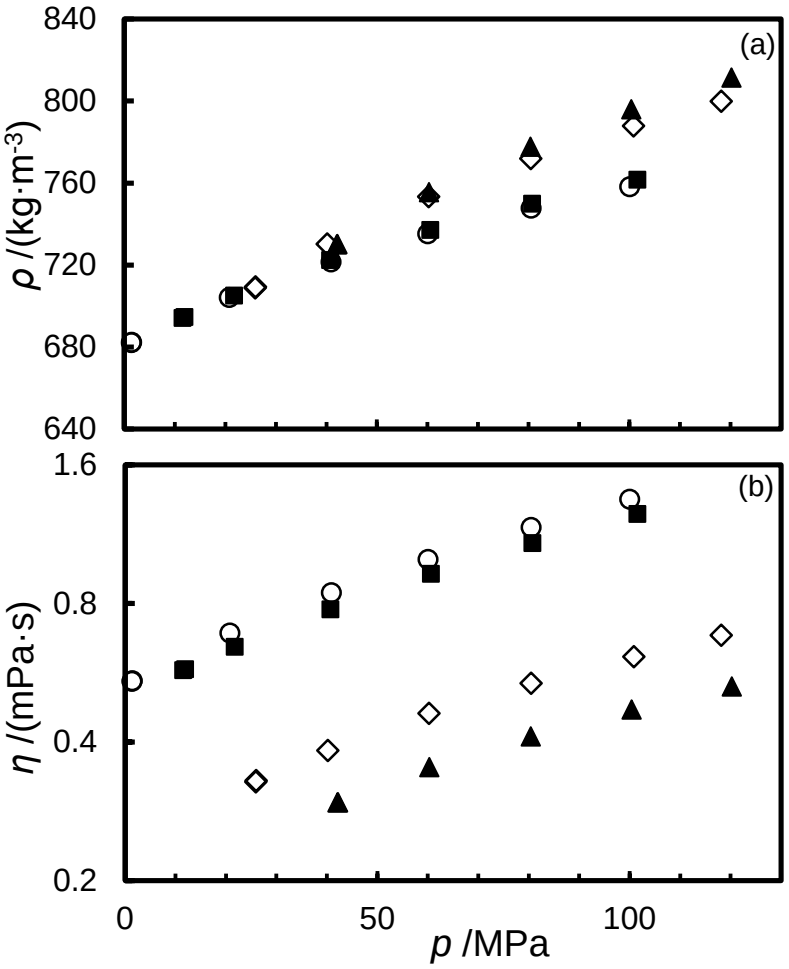

Figure 8.

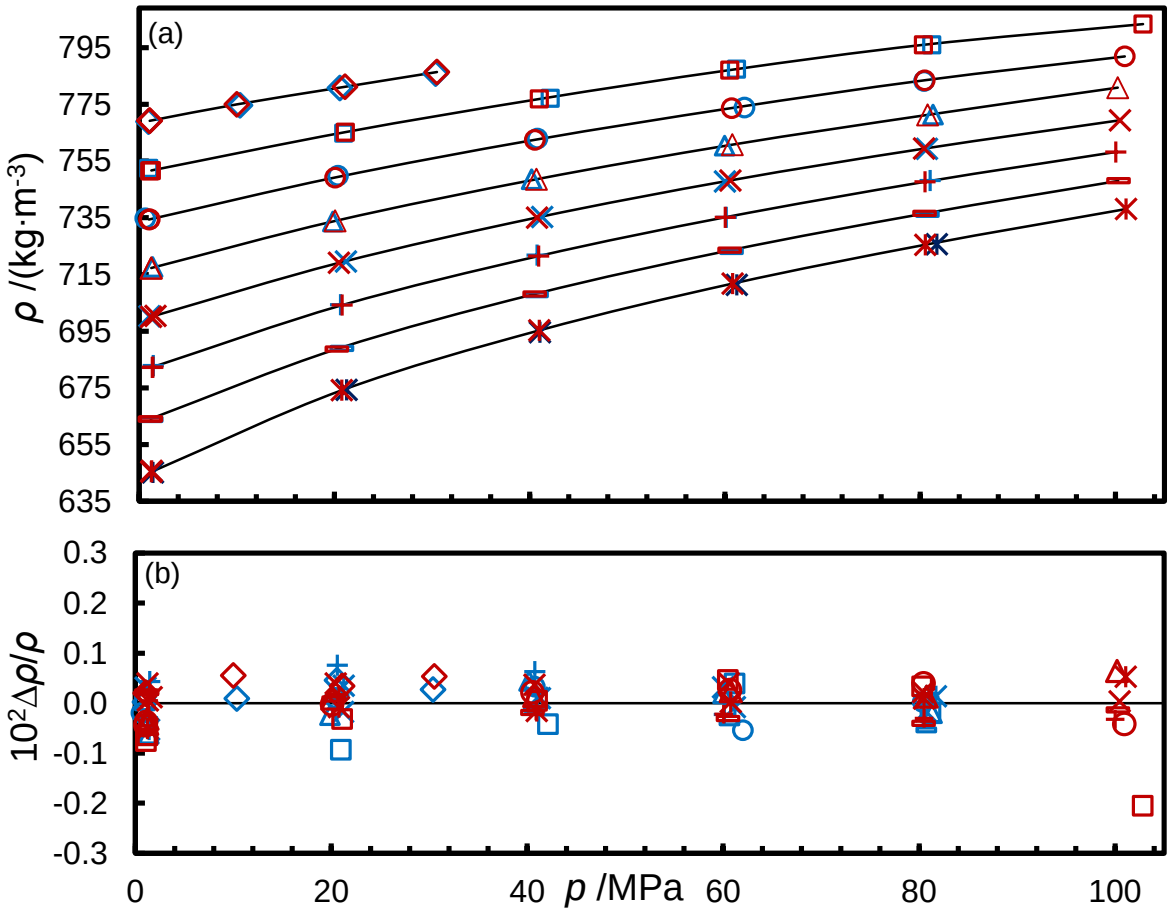
(a)
795
775
755
735
715
695
675
655
635
ρ /(kg·m-3)
(b)
0.3
0.2
0.1
0.0
-0.1
-0.2
-0.3
10²Δρ/ρ
0
20
40
60
80
100
p /MPa

Figure 9.

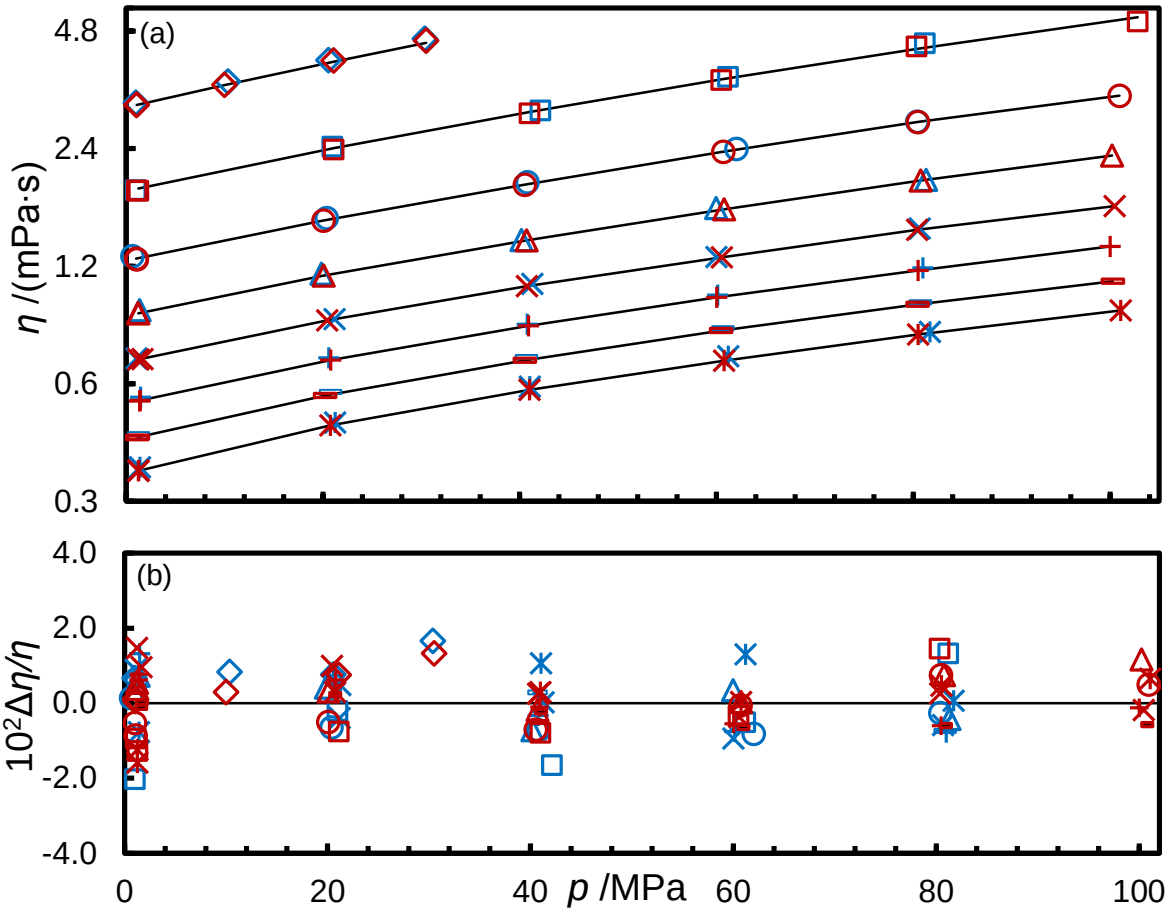

Figure 10.

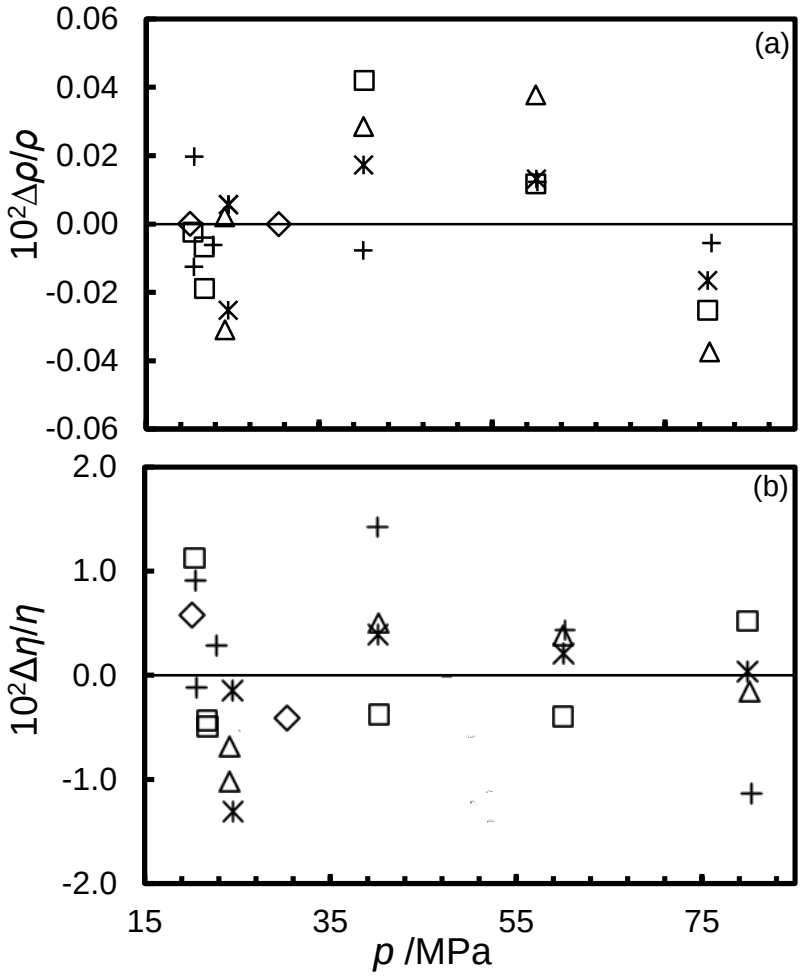
(a)
(b)
0.06
0.04
0.02
0.00
-0.02
-0.04
-0.06
2.0
1.0
0.0
-1.0
-2.0
15
35
55
75
$10^2\Delta\rho/\rho$
$10^2\Delta\eta/\eta$
p /MPa

Figure 11.

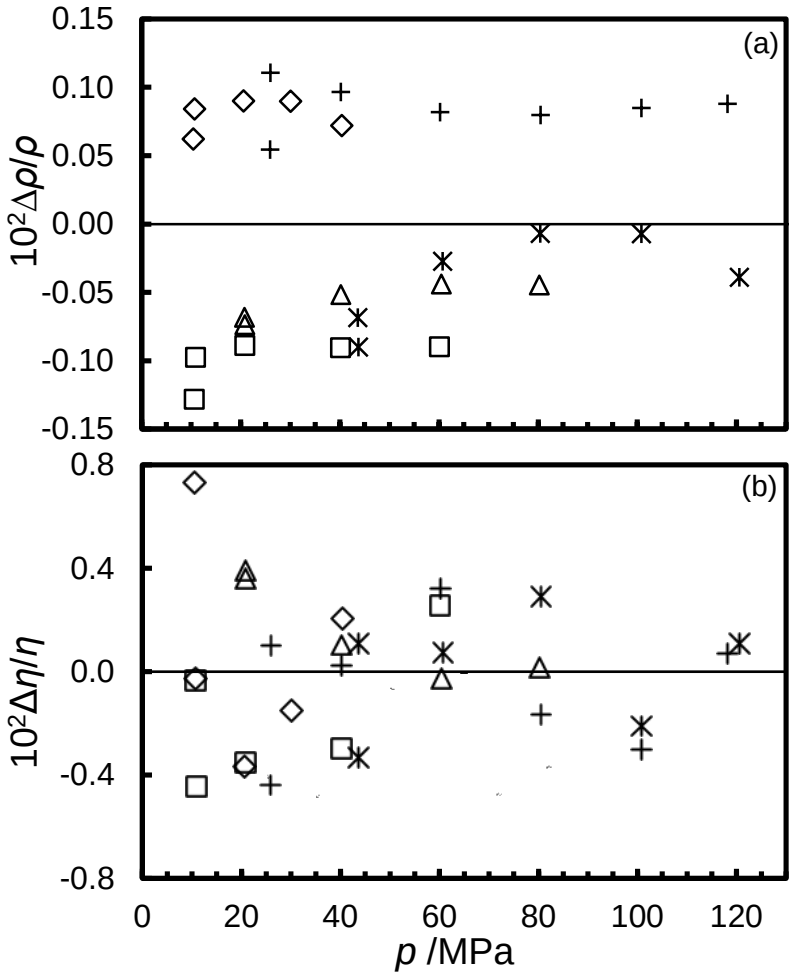
(a)
(b)
0.15
0.10
0.05
0.00
-0.05
-0.10
-0.15
0.8
0.4
0.0
-0.4
-0.8
0
20
40
60
80
100
120
$10^2\Delta\rho/\rho$
$10^2\Delta\eta/\eta$
p /MPa

Figure 12.

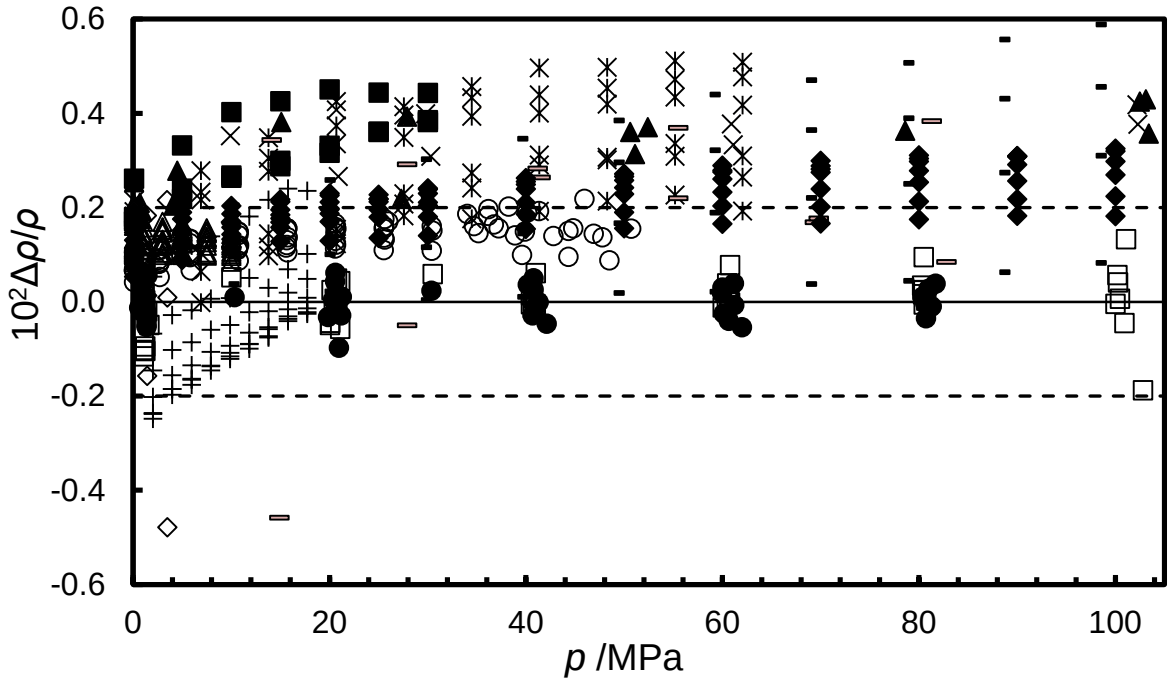

Figure 13.

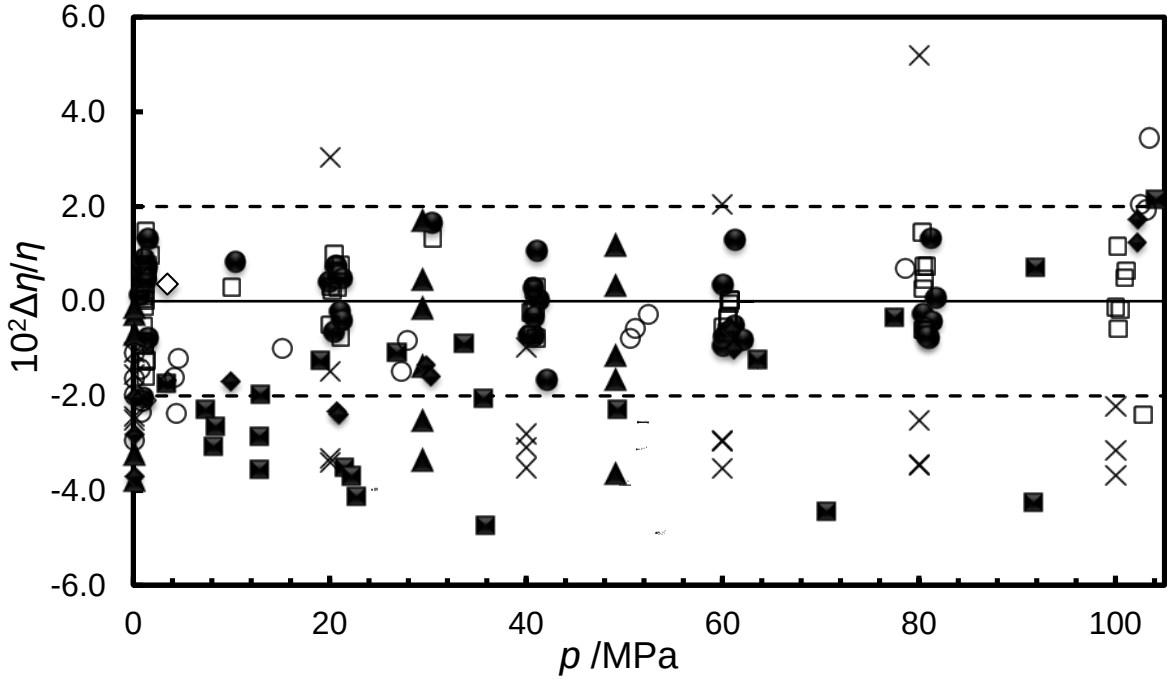

Figure 14.

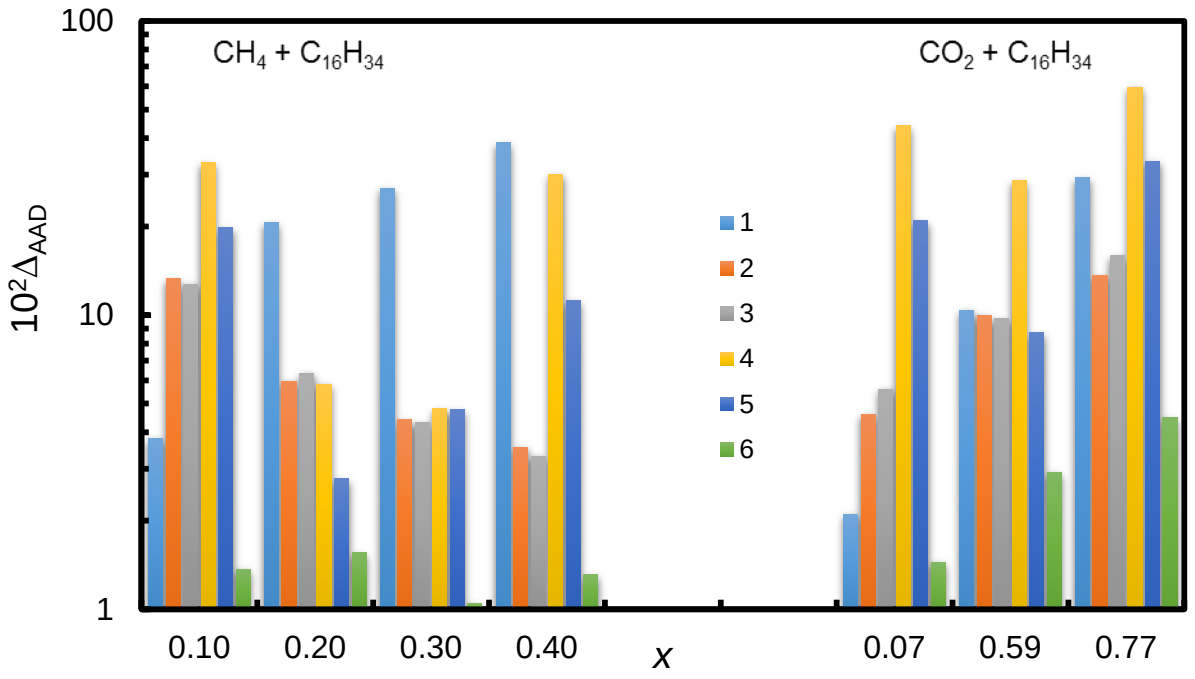

Figure 15.

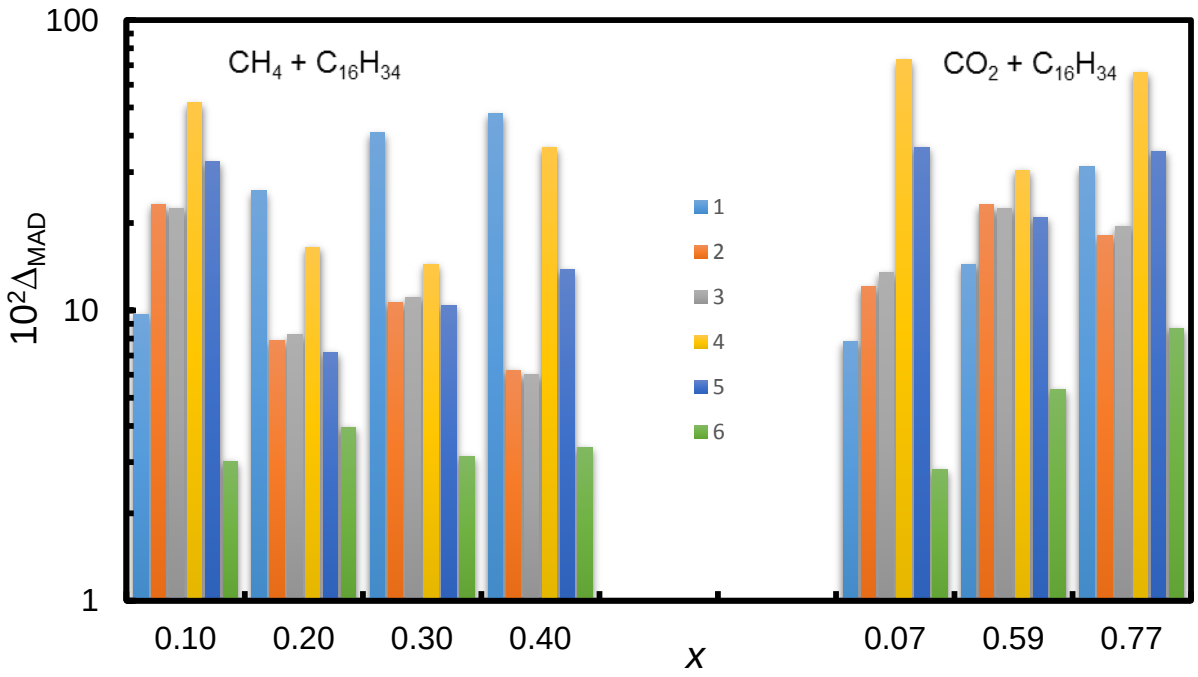

Figure 16.

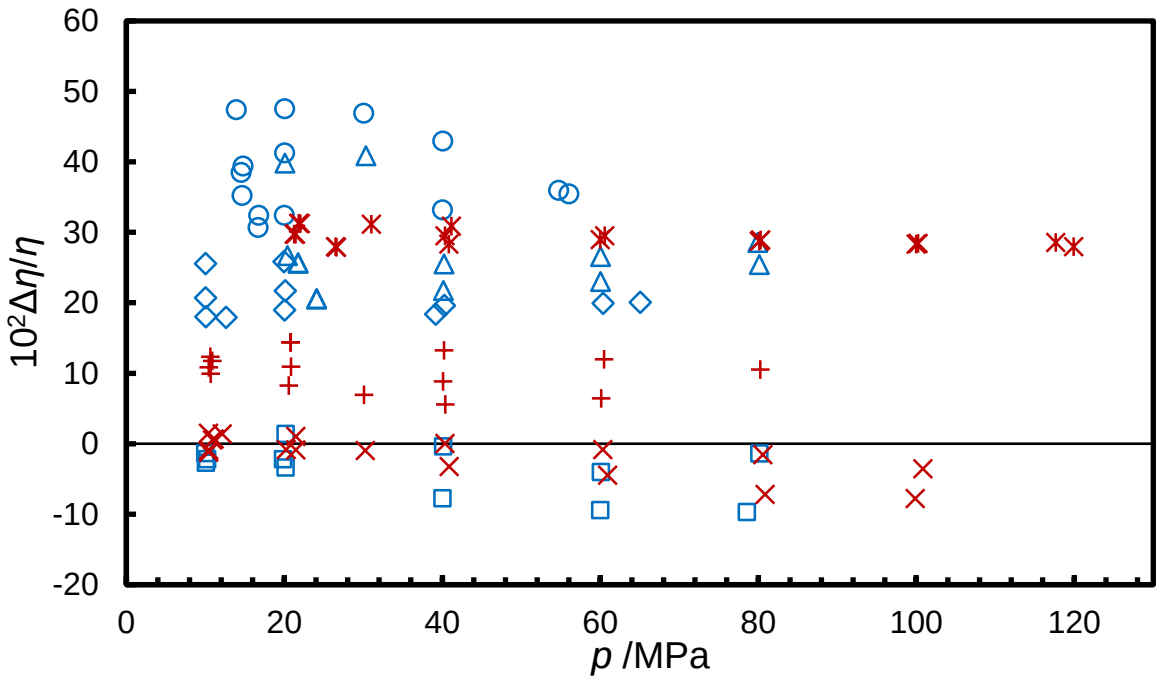

Figure 17.

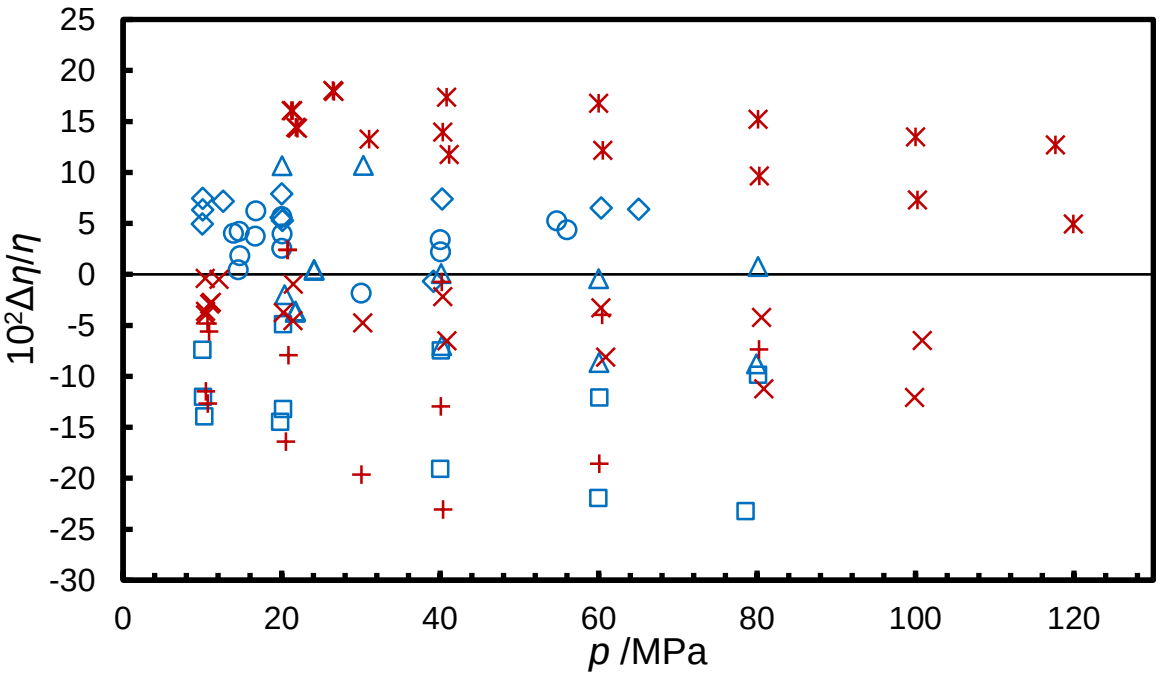

Figure 18.

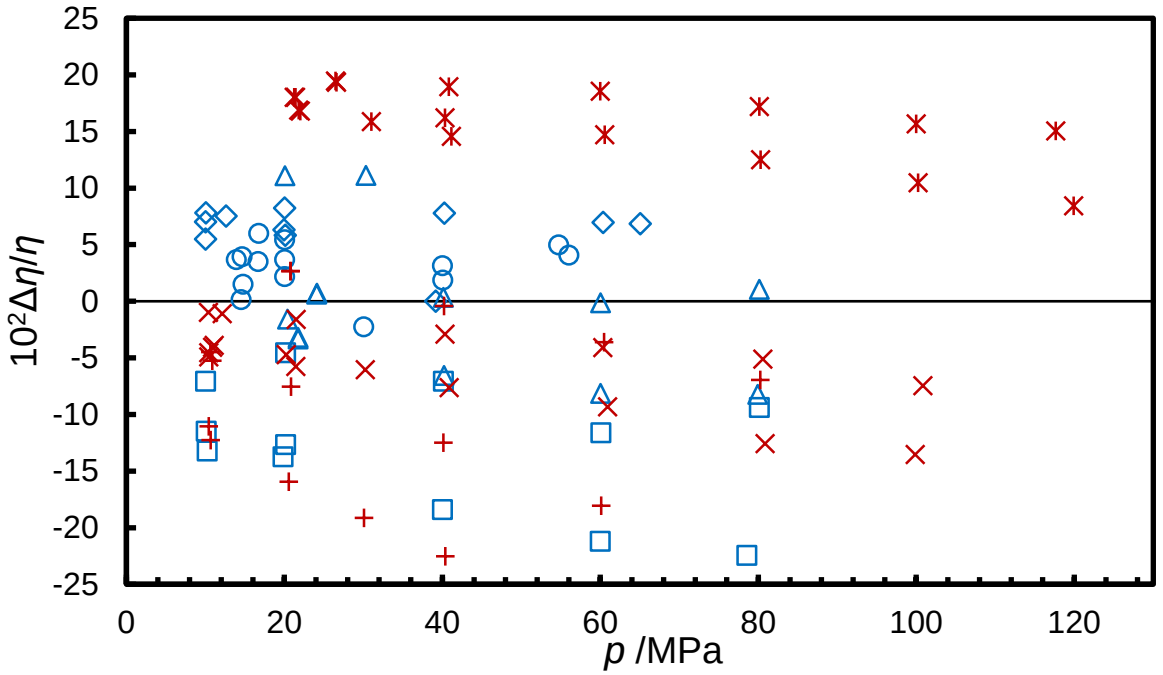

Figure 19.

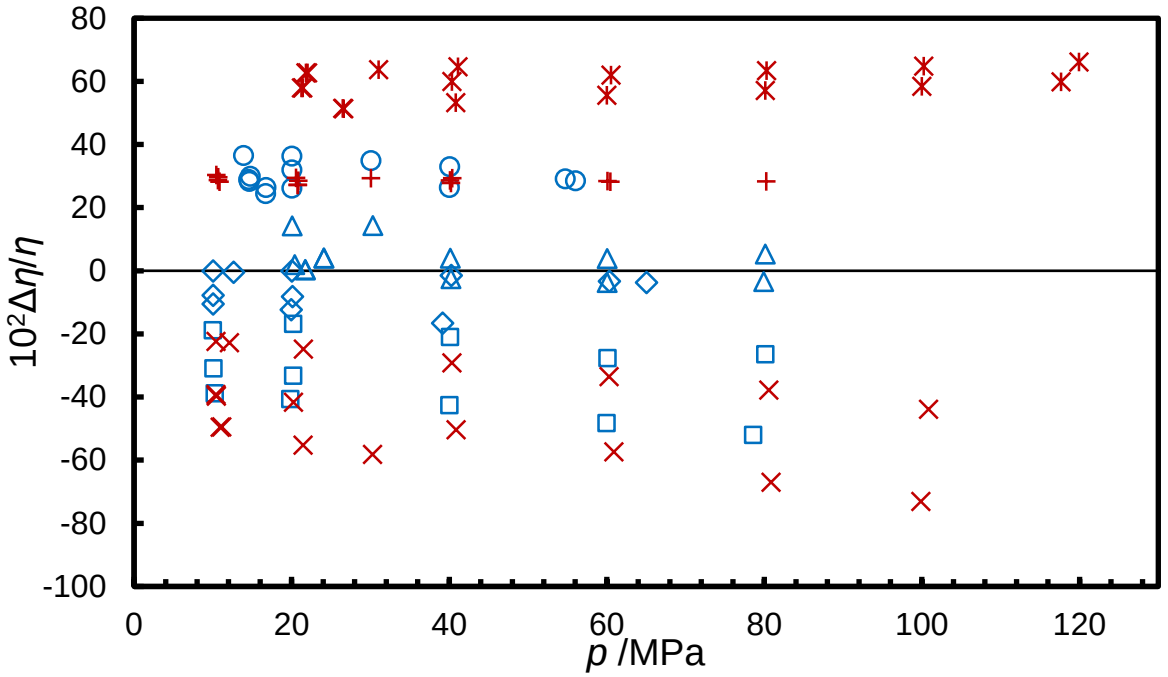

Figure 20.

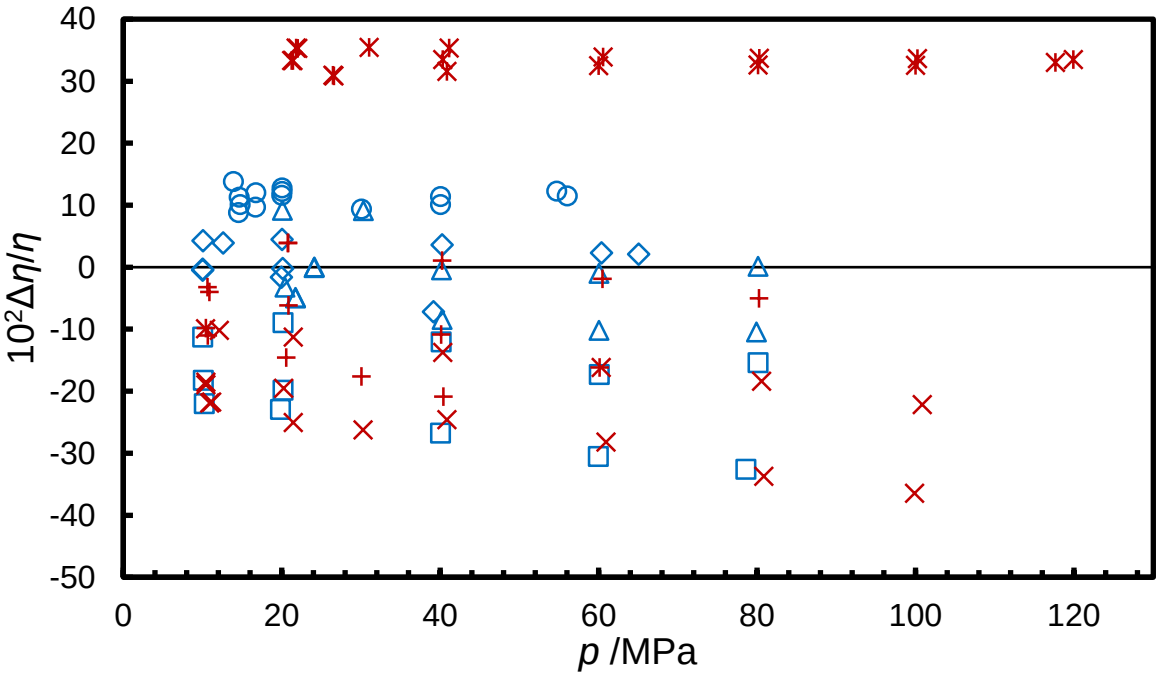

Figure 21.

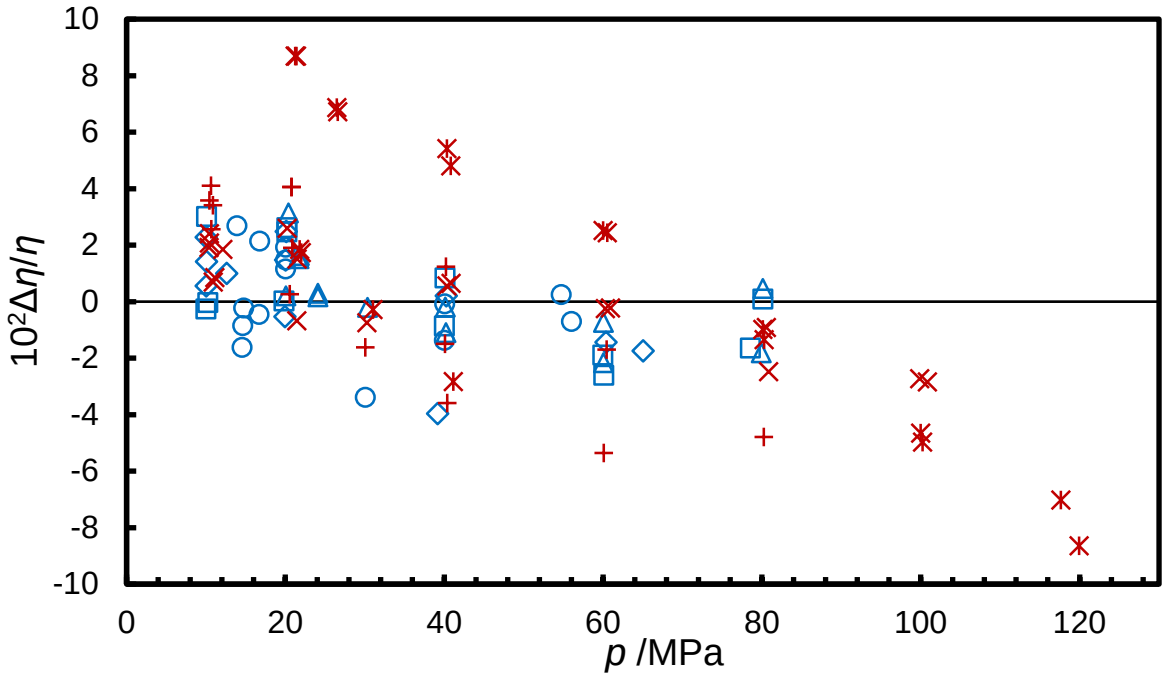

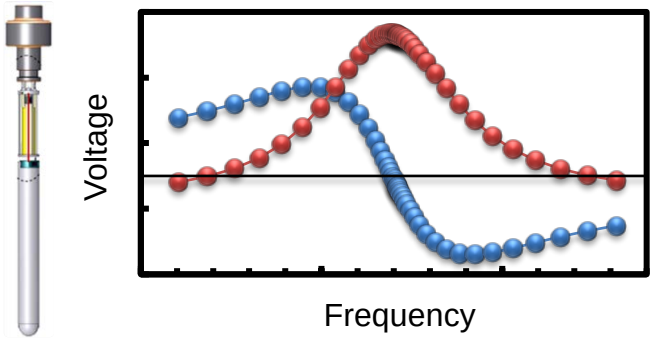

For Table of Contents Only.)